Article

Cell Reports

Lsd1 Ablation Triggers Metabolic Reprogramming of Brown Adipose Tissue

Graphical Abstract

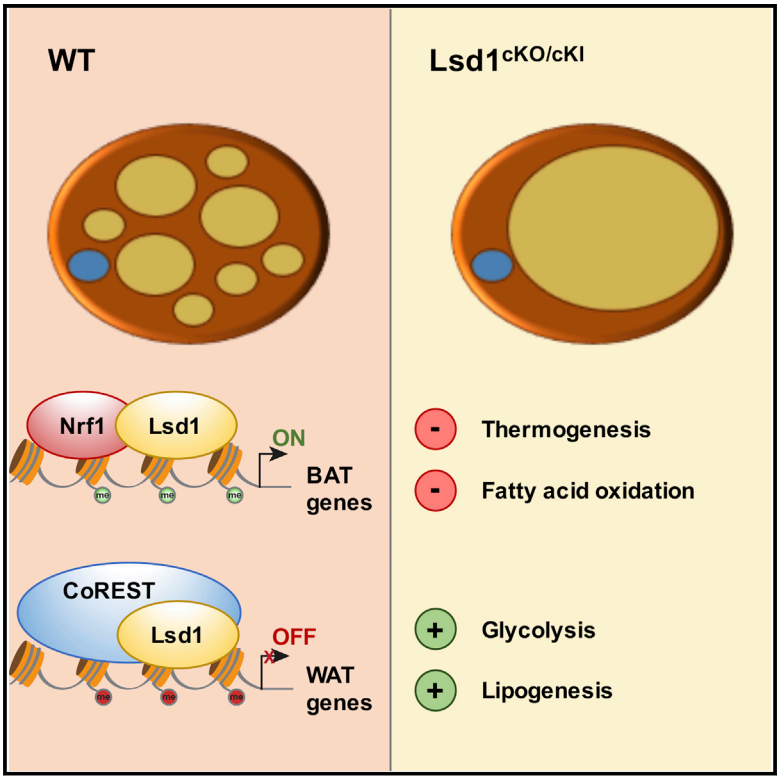

Authors

Delphine Duteil, Milica Tosic, Franziska Lausecker, ..., Jörn Dengjel, Toufike Kanouni, Roland Schüle

Correspondence

roland.schuele@uniklinik-freiburg.de

In Brief

Duteil et al. find that BAT-selective Lsd1 ablation downregulates BAT-selective and upregulates WAT-selective gene expression. Lsd1 deletion shifts oxidative to glycolytic metabolism, resulting in whitening of BAT. Lsd1 maintains BAT properties in concert with the transcription factor Nrf1 and CoREST.

Highlights

- Loss of Lsd1 in brown adipocytes induces a brown-to-white fat cell conversion
- Lsd1 controls BAT- and WAT-selective genes via a dual mechanism
- Lsd1 deletion in brown adipocytes shifts oxidative to glycolytic metabolism
- Lsd1 controls thermogenesis in BAT to counteract obesity

Accession Numbers

GSE81557
GSE81557
PXD004745

Duteil et al., 2016, Cell Reports *17*, 1008–1021
October 18, 2016
http://dx.doi.org/10.1016/j.celrep.2016.09.053

CellPress

OPEN ACCESS
CellPress

Cell Reports
Article

Lsd1 Ablation Triggers Metabolic Reprogramming of Brown Adipose Tissue

Delphine Duteil,[1] Milica Tosic,[1] Franziska Lausecker,[1] Hatice Z. Nenseth,[1] Judith M. Müller,[1] Sylvia Urban,[1] Dominica Willmann,[1] Kerstin Petroll,[1,2] Nadia Messaddeq,[3] Laura Arrigoni,[4] Thomas Manke,[4] Jan-Wilhelm Kornfeld,[5] Jens C. Brüning,[5] Vyacheslav Zagoriy,[6] Michael Meret,[6] Jörn Dengjel,[7] Toufike Kanouni,[8] and Roland Schüle[1,9,10,11,*]
[1]Urologische Klinik und Zentrale Klinische Forschung, Klinikum der Universität Freiburg, Breisacherstrasse 66, 79106 Freiburg, Germany
[2]Center for Biological Systems Analysis, 79106 Freiburg, Germany
[3]IGBMC, Department of Functional Genomics and Cancer, Inserm U964, CNRS UMR7104, Université de Strasbourg, 67404 Illkirch, France
[4]Max Planck Institute of Immunobiology and Epigenetics, Stübeweg 51, Freiburg 79108, Germany
[5]Max Planck Institute for Metabolism Research, 50931 Cologne, Germany
[6]metaSysX GmbH, Am Mühlenberg 11, 14476 Potsdam-Golm, Germany
[7]Department of Biology, Université de Fribourg, Chemin du Musée 10, 1700 Fribourg, Switzerland
[8]Celgene Quanticel Research, 9393 Towne Centre Dr., Suite 110, San Diego, CA 92121, USA
[9]BIOSS Centre of Biological Signalling Studies, Albert Ludwigs University, 79106 Freiburg, Germany
[10]Deutsches Konsortium für Translationale Krebsforschung (DKTK), Standort Freiburg, 79108 Freiburg, Germany
[11]Lead Contact
*Correspondence: roland.schuele@uniklinik-freiburg.de
http://dx.doi.org/10.1016/j.celrep.2016.09.053

SUMMARY

Previous work indicated that lysine-specific demethylase 1 (Lsd1) can positively regulate the oxidative and thermogenic capacities of white and beige adipocytes. Here we investigate the role of Lsd1 in brown adipose tissue (BAT) and find that BAT-selective Lsd1 ablation induces a shift from oxidative to glycolytic metabolism. This shift is associated with downregulation of BAT-specific and upregulation of white adipose tissue (WAT)-selective gene expression. This results in the accumulation of di- and triacylglycerides and culminates in a profound whitening of BAT in aged Lsd1-deficient mice. Further studies show that Lsd1 maintains BAT properties via a dual role. It activates BAT-selective gene expression in concert with the transcription factor Nrf1 and represses WAT-selective genes through recruitment of the CoREST complex. In conclusion, our data uncover Lsd1 as a key regulator of gene expression and metabolic function in BAT.

INTRODUCTION

Adipose tissue is an important metabolic regulator of energy balance (Langin, 2010). In mammals, three types of adipose tissues exist. White adipose tissue (WAT) is essentially composed of white adipocytes containing one single large lipid vesicle. WAT is mainly located in the abdominal and subcutaneous areas of the body and is highly adapted to store excess energy in the form of triacylglycerides. Conversely, beige and brown adipocytes are highly energy-expending (Lee et al., 2014a). They are able to dissipate energy in the form of heat via the action of uncoupling protein-1 (Ucp1) (Tiraby and Langin, 2003). Brown adipocytes reside in discrete brown adipose tissue (BAT) depots, such as the interscapular area in rodents, whereas beige adipocytes are intermingled with white adipocytes in WAT. Both brown and beige adipocytes have a multilocular morphology and large numbers of mitochondria and express a common set of brown/beige fat-selective genes, including Ucp1 (Lee et al., 2014b). In rodents, heat generated by brown or beige adipocytes via Ucp1 is essential to survive the cold season (Cohen and Spiegelman, 2015). In both cell types, the cold response is mainly regulated by the sympathetic nervous system, in particular by the β3-adrenergic signaling pathway (Cannon and Nedergaard, 2004). In addition to its role in thermogenesis and fatty acid oxidation, it has been reported that BAT activated by the β3-adrenergic signaling pathway can improve glucose homeostasis (Peirce and Vidal-Puig, 2013).

Because recent studies have shown that brown/beige adipocytes exist in quantifiable amounts in humans (Betz and Enerbäck, 2015), these fat types have been rediscovered as potential therapeutic targets for weight loss. Therefore, understanding brown/beige adipocyte function and finding new ways to modulate their activity has become a major scientific point of interest (Betz and Enerbäck, 2015). Among other factors (Harms et al., 2014; Kleiner et al., 2012; Puigserver et al., 1998; Vernochet et al., 2012), the epigenetic regulator lysine-specific demethylase 1 (Lsd1) (Cai et al., 2014; Metzger et al., 2005, 2016), a flavin adenine dinucleotide (FAD)-dependent amine oxidase, has been shown to regulate the differentiation and function of white and beige adipocytes (Duteil et al., 2014; Musri et al., 2010). In WAT, Lsd1 is induced by cold and involved in mediating the effects of β3-adrenergic signaling. Notably, we recently demonstrated that increased expression of Lsd1 in mouse WAT promotes the development of thermogenically active beige adipocytes and suppresses metabolic disorders such as obesity and type 2 diabetes (Duteil et al., 2014). Moreover, in mature white adipocytes, elevation of Lsd1 levels is sufficient to activate mitochondria biogenesis, oxidative phosphorylation, and

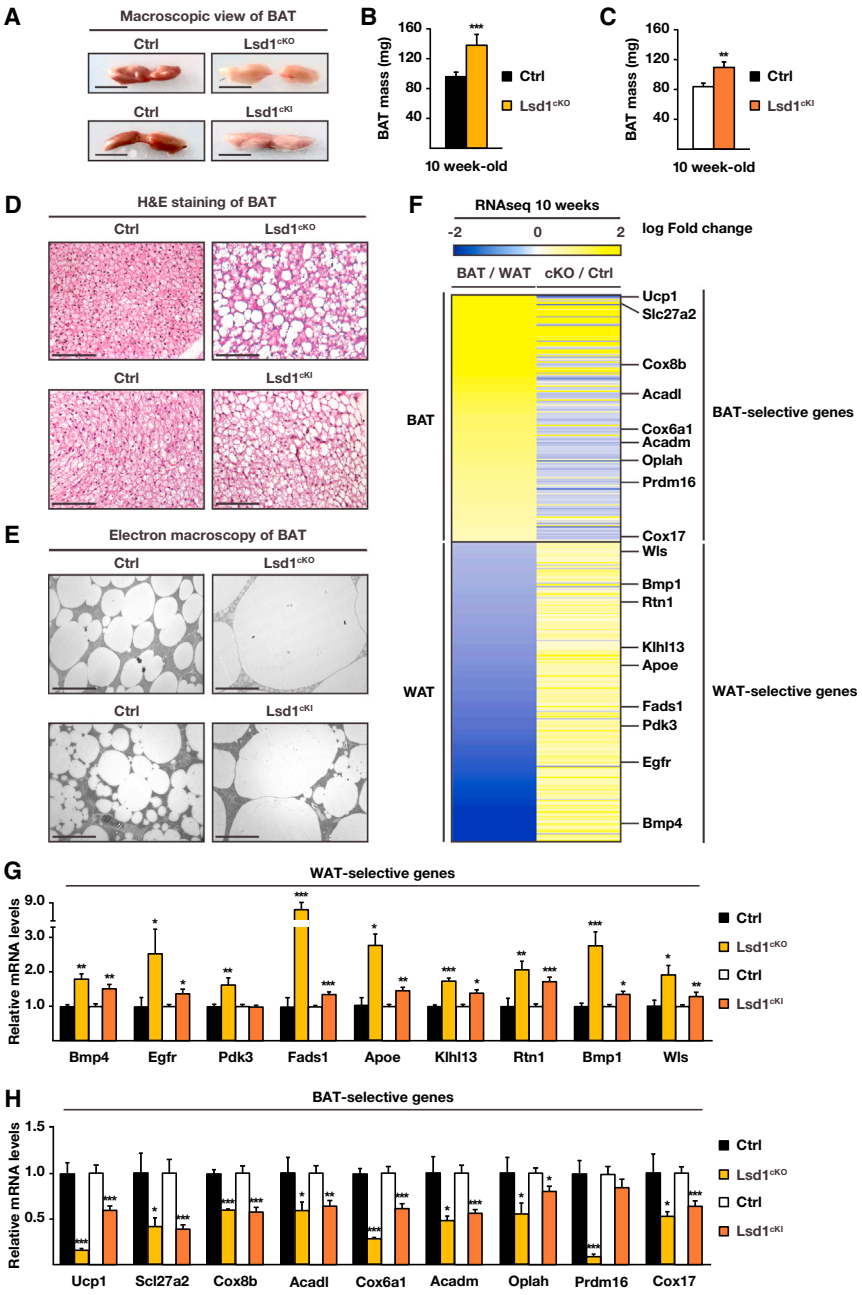

Figure 1. Lsd1 Represses the Expression of WAT-Selective Genes in BAT

(A–E) Macroscopic view (A), mass (B and C), H&E staining (D), and ultrastructure analysis (E) of representative sections of BAT of control (Ctrl), Lsd1^{cKO}, and Lsd1^{cKI} mice.

(B and C) Mean + SEM, **p < 0.01, ***p < 0.001.

(B) Ctrl, n = 9; Lsd1^{cKO}, n = 7.

(C) Ctrl, n = 7; Lsd1^{cKI}, n = 6.

(F) Heatmap comparing mRNA levels of BAT- and WAT-selective genes in BAT and WAT of control mice (BAT/WAT) and in BAT of Lsd1^{cKO} and control mice (cKO/Ctrl) at 10 weeks of age (Ctrl, n = 4; Lsd1^{cKO}, n = 4).

(G and H) Relative mRNA levels of WAT-selective (G) and BAT-selective (H) genes in BAT of control, Lsd1^{cKO}, and Lsd1^{cKI} mice (mean + SEM, *p < 0.05, **p < 0.01, ***p < 0.001; Ctrl [black bars], n = 9; Lsd1^{cKO} [orange bars], n = 7; Ctrl [white bars], n = 7; Lsd1^{cKI} [red bars], n = 6).

Scale bars, 5 mm (A), 100 μm (D), 10 μm (E). See also Figure S1 and Table S1.

thermogenesis (Duteil et al., 2014). In contrast, the role of Lsd1 in BAT has not been investigated in detail. Brown fat cells exhibit a gene expression profile distinct from either beige or white adipocytes (Wu et al., 2012). Because Lsd1 is a key regulator of metabolism in mature white or beige adipocytes, we asked whether Lsd1 might also play a role in controlling brown adipocyte function.

In this study, we show that selective ablation of Lsd1 or inactivation of its catalytic activity in brown adipocytes triggers a profound whitening of BAT. Lsd1 loss and genetic or chemical inhibition elicits a dramatic rise in expression of WAT-selective genes while impairing the expression of BAT-selective genes. Our data demonstrate that Lsd1 acts via a dual mechanism by positively regulating the expression of BAT-selective genes in cooperation with Nrf1 and actively repressing the expression of WAT-selective genes in concert with the CoREST complex. The whitening of BAT observed upon depletion or inhibition of Lsd1 is accompanied by a shift from oxidative to glycolytic metabolism associated with an accumulation of di- and triacylglycerides. This collapse of BAT function accelerates body weight gain but improves glucose tolerance. Taken together, our results demonstrate that Lsd1 is essential to maintain the metabolic function of brown adipose tissue.

RESULTS

Lsd1 Represses the White Fat Program in Brown Adipose Tissue

To investigate the role of Lsd1 in BAT, we crossed mice harboring conditional *Lsd1* alleles (Zhu et al., 2014) with the *Ucp1-Cre* deleter strain (Turpin et al., 2014), which resulted in Cre-mediated loss of Lsd1 selectively in brown and beige adipocytes (*Lsd1*$^{Ucp1\text{-}Cre}$, hereafter named Lsd1^{cKO}) (Figures S1A and S1B). At 10 weeks of age, Lsd1^{cKO} mice exhibited a profound morphological whitening of their BAT (Figure 1A). This whitening was accompanied by an ~40% increase in tissue mass (Figure 1B), a switch from multilocular to unilocular morphology, and increased lipid content (Figures 1D and 1E). In Lsd1^{cKO} mice, the morphology of mitochondria was severely altered with substantially augmented size and less densely packed cristae (Figure S1C). In accordance, the DNA content of mitochondria was decreased by

around 60% in Lsd1^{cKO} mice (Figure S1D), indicating degradation and dysfunction of this organelle. These observations suggested that loss of Lsd1 in brown adipocytes shifted BAT toward a white fat-like phenotype.

Accordingly, we expected to see changes in the transcriptional program of brown adipocytes of Lsd1^{cKO} mice that resemble the gene expression profile observed in white adipocytes. We therefore determined the transcriptome of Lsd1-deleted BAT and compared it with the transcriptome of WAT of control mice, which was described previously (Fitzgibbons et al., 2011; Figure 1F; Table S1). The vast majority of WAT-selective genes (95%) was upregulated in BAT of Lsd1^{cKO} mice, whereas 67% of BAT-selective genes showed reduced expression (Figure 1F; Table S1). qRT-PCR analysis confirmed that the white fat transcriptome was enhanced to the detriment of the brown fat program, as illustrated by significantly increased expression of representative WAT-selective genes such as *Bmp4*, *Egfr*, *Pdk3*, *Fads1*, *Apoe*, *Klhl13*, *Rtn1*, *Bmp1*, and *Wls* (Figure 1G) and decreased expression of representative BAT-selective genes (*Ucp1*, *Slc27a2*, *Cox8b*, *Acadl*, *Cox6a1*, *Acadm*, *Oplah*, *Prdm16*, and *Cox17*) (Figure 1H) in Lsd1^{cKO} mice. In line with these RNA expression data, western blot analyses showed that BAT of Lsd1^{cKO} mice expressed higher levels of Apoe and reduced levels of Ucp1 protein (Figure S1E). These data suggest that, in BAT, Lsd1 is required to repress the expression of white fat-selective genes while supporting the brown fat-selective gene expression program.

Lsd1 Demethylase Activity Is Required to Maintain the Gene Expression Program of BAT in Mice

To determine whether Lsd1 demethylase activity is required to maintain the brown fat program, we engineered mice homozygous for a conditional, enzymatically inactive mutant *Lsd1* knockin allele (*Lsd1*$^{KI/KI/Ucp1\text{-}Cre}$, hereafter named Lsd1^{cKI}) (Figures S1F–S1I). In BAT of these mice, the endogenous Lsd1 gene is replaced by an enzymatically inactive Lsd1 mutant allele following *Ucp1-Cre*-mediated recombination. As observed in Lsd1-depleted mice, we found that BAT of Lsd1^{cKI} mice was increased in size and contained a large proportion of unilocular adipocytes (Figures 1A and 1C–1E). Although Lsd1 mRNA levels remained unchanged (Figure S1H), the expression levels of WAT-selective genes were increased, whereas the levels of BAT-selective genes were decreased (Figures 1G and 1H; Figure S1I). In conclusion, alterations in BAT morphology and transcription pattern in Lsd1^{cKI} mice resemble those of Lsd1^{cKO} mice, demonstrating that Lsd1 demethylase activity contributes to the phenotype observed in genetically modified mice.

Because the expression of Ucp1 is initiated in utero between embryonic day (E) 18.5 and E19.5, Lsd1 ablation by *Ucp1-Cre*-mediated recombination is expected to occur around birth (Giralt et al., 1990). To investigate the role of Lsd1 in adult BAT, 10-week-old wild-type mice were treated for 5 days with the Lsd1-specific nanomolar affinity inhibitor QC6688 (Lsd1(i)) or vehicle. BAT of mice treated with Lsd1(i) showed a profoundly pale color and increased size compared with that of vehicle-treated mice (Figure 2A; Figure S2A). H&E staining of BAT sections revealed that Lsd1(i)-treated adipocytes had larger lipid droplets compared with those of vehicle-treated mice (Figure 2B). The expression levels of representative WAT-selective genes were increased at both mRNA and protein levels (Figures 2C and 2E), whereas expression of representative BAT-selective genes was decreased in QC6688-treated mice (Figures 2D and 2E). These data corroborate our findings in Lsd1^{cKI} mice and suggest that catalytically active Lsd1 is required to maintain the metabolic properties of BAT.

To investigate the cell autonomy of Lsd1(i) in BAT, we treated differentiated primary brown adipocytes (hereafter named brown adipocytes) isolated from the stromal vascular fraction with Lsd1(i) or vehicle for 3 days. As shown by oil red O staining, Lsd1(i)-treated brown adipocytes accumulated more fat than vehicle-treated cells (Figure 2F) and shifted their transcription pattern to a white adipocyte-like program (Figures S2B–S2D). Together, these data demonstrate that the gene expression program of brown adipocytes is controlled by the catalytic activity of Lsd1 in a cell-autonomous manner.

Lsd1 Has a Dual Role in Controlling Expression of BAT- and WAT-Selective Genes

Next we determined genome-wide Lsd1 chromatin occupancy in brown adipocytes by chromatin immunoprecipitation using Lsd1 antibody followed by massive parallel sequencing (ChIP-seq). The antibody was validated previously and specifically recognizes Lsd1 (Duteil et al., 2014). We found that Lsd1 occupied the promoter of 75% of the BAT-selective genes (103 genes) and 68% of the WAT-selective genes (158 genes) differentially regulated in Lsd1^{cKO} mice (Figure 2G), suggesting a dual mechanism by which Lsd1 represses the expression of WAT-selective genes while activating that of BAT-selective genes.

Hypergeometric optimization of motif enrichment (HOMER) motif searches revealed that promoter occupancy of Lsd1 significantly correlated with the presence of binding sites for the transcription factors Nrf1 and Rest (Figure 2H). Thus, we hypothesized that Lsd1 might positively regulate BAT-selective genes in cooperation with Nrf1 while repressing WAT-selective gene expression in concert with the CoREST complex. ChIP with Nrf1 antibody followed by qPCR analysis in brown adipocytes showed that Lsd1 and Nrf1 co-localized at promoters of representative BAT-selective genes such as *Acadm*, *Oplah*, and *Cox6a1* (Figure 3A). *Ucp1* was not part of the analysis because our genome-wide cistrome analysis by ChIP-seq showed no Lsd1 occupancy. Importantly, Nrf1 was not present at the promoter of WAT-selective genes, as illustrated by Figure S3A. Because Lsd1 is known to activate gene expression by erasing dimethyl groups at lysine 9 of histone 3 (H3K9me2), we hypothesized that inhibition of Lsd1 would modify methylation levels of H3K9 at BAT-selective genes. ChIP-qPCR analysis for H3K9me2 revealed that levels of H3K9me2 were increased upon Lsd1(i) treatment at promoters of BAT-selective genes (Figure 3B). In parallel, levels of H3K4me2 were reduced in Lsd1(i)-treated cells (Figure S3B), indicating a repressive transcriptional context. To investigate whether Lsd1 and Nrf1 are present in the same protein complex, nuclear extracts from brown adipocytes were subjected to size exclusion chromatography. Western blot analysis showed that Lsd1 and Nrf1 co-fractionate, suggesting the existence of an Nrf1/Lsd1complex (Figure S3C). Furthermore, Lsd1 and Nrf1 co-immunoprecipitated, confirming interaction

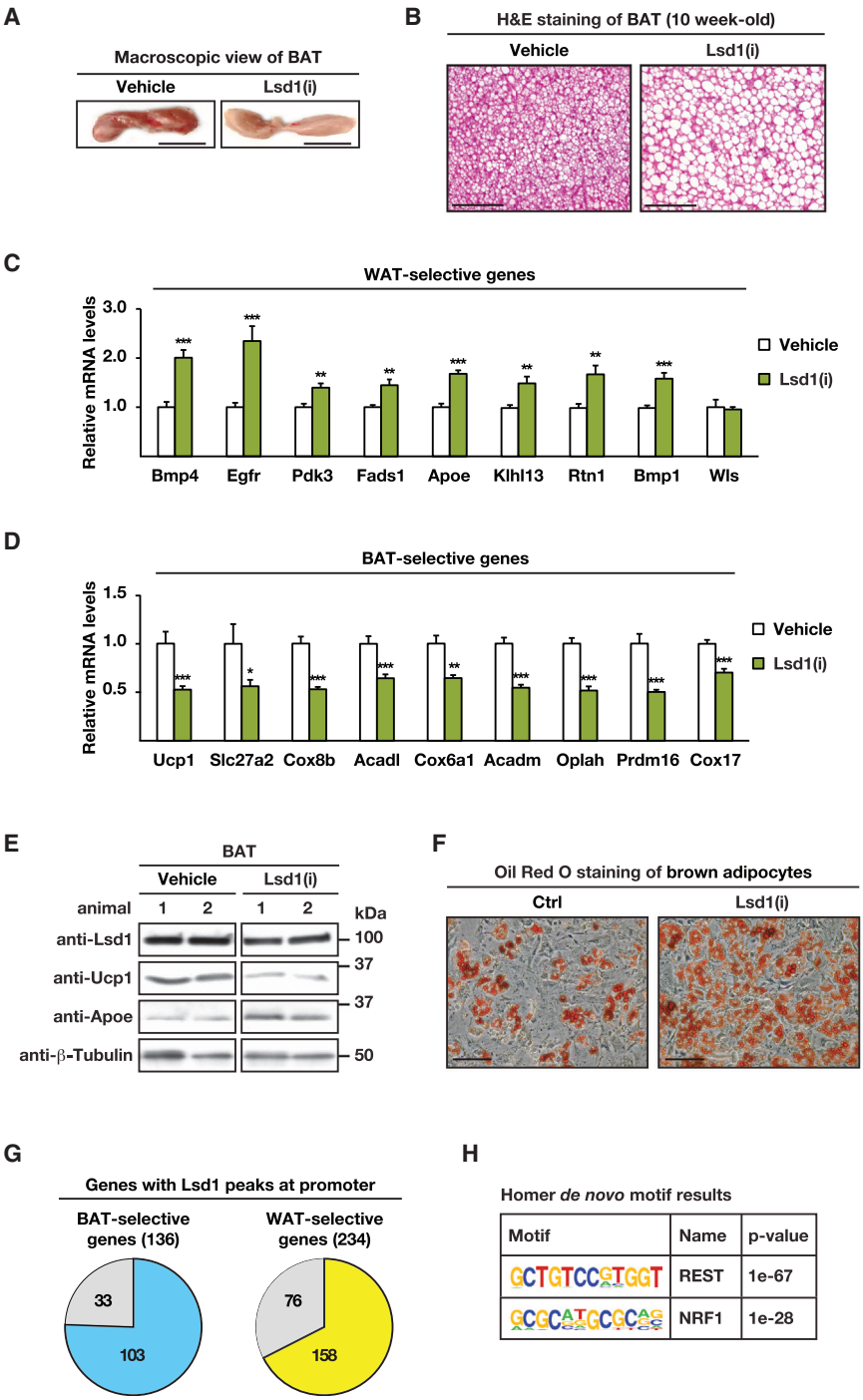

Figure 2. The Demethylase Activity of Lsd1 Is Required to Maintain BAT Properties

(A and B) Macroscopic view (A) and H&E staining (B) of representative sections of BAT of mice treated with vehicle or Lsd1(i).

(C and D) Relative mRNA levels of WAT-selective (C) and BAT-selective (D) genes in BAT of mice treated with vehicle or Lsd1(i) (mean + SEM, *$p < 0.05$, **$p < 0.01$, ***$p < 0.001$; vehicle, $n = 6$; Lsd1(i), $n = 7$).

(E) Western blot analysis of Lsd1, Ucp1, and Apoe in BAT of mice treated with vehicle or Lsd1(i). β-Tubulin was used as a loading control.

(F) Oil red O staining of differentiated primary brown adipocytes treated with vehicle or Lsd1(i).

(G) Pie chart depicting BAT- and WAT-selective genes with Lsd1 peaks at promoters in differentiated primary brown adipocytes.

(H) HOMER motif analysis of Lsd1 ChIP-seq data unraveled Rest and Nrf1 binding sites among the top-scoring motifs.

Scale bars, 5 mm (A), 100 μm (B), 50 μm (F). See also Figure S2.

between these two endogenously expressed proteins in BAT (Figure S3D). Accordingly, small interfering RNA (siRNA)-mediated knockdown of Nrf1 (Figure S3E) significantly decreased transcript levels of BAT-selective genes but did not impair WAT-selective gene expression (Figure 3C). Together, these data demonstrate that Lsd1 controls the expression of BAT-selective genes in cooperation with Nrf1 by targeting H3K9 methylation levels.

Next we analyzed whether an Lsd1-associated repressor complex might regulate the WAT-selective gene program in BAT. For this purpose, nuclear protein extracts from BAT were used for immunoprecipitation with three distinct anti-Lsd1 antibodies directed against various Lsd1 domains followed by liquid chromatography-tandem mass spectrometry (LC-MS/MS). The intersection of the three interactomes uncovered 163 proteins commonly interacting with Lsd1 (Figure S3F) and revealed the repressive CoREST complex as a significantly enriched protein group (Table S2). Interaction between Lsd1 and CoREST has already been well established (Lee et al., 2005; Metzger et al., 2005; Shi et al., 2004). Accordingly, co-immunoprecipitation experiments and size exclusion chromatography demonstrated that, also in BAT, endogenous Lsd1 interacts with members of the CoREST complex (Figures S3G and S3H). To test whether the CoREST complex indeed represses the expression of WAT-selective genes, we knocked down the complex members Rcor1 and Rcor3 in brown adipocytes (Figure S3I). Cells treated with Rcor1 or Rcor3 siRNA upregulated WAT-selective genes (Figure 3D) without affecting BAT-selective genes, as exemplified by *Oplah* and *Acadl* (Figure 3D), and accumulated more lipids than cells treated with control siRNA (Figure S3J). In addition, ChIP-qPCR analyses confirmed the colocalization of Rcor1 and Rcor3 with Lsd1 specifically at promoters of WAT-selective genes (Figure 3E) but not at promoters of BAT-selective genes

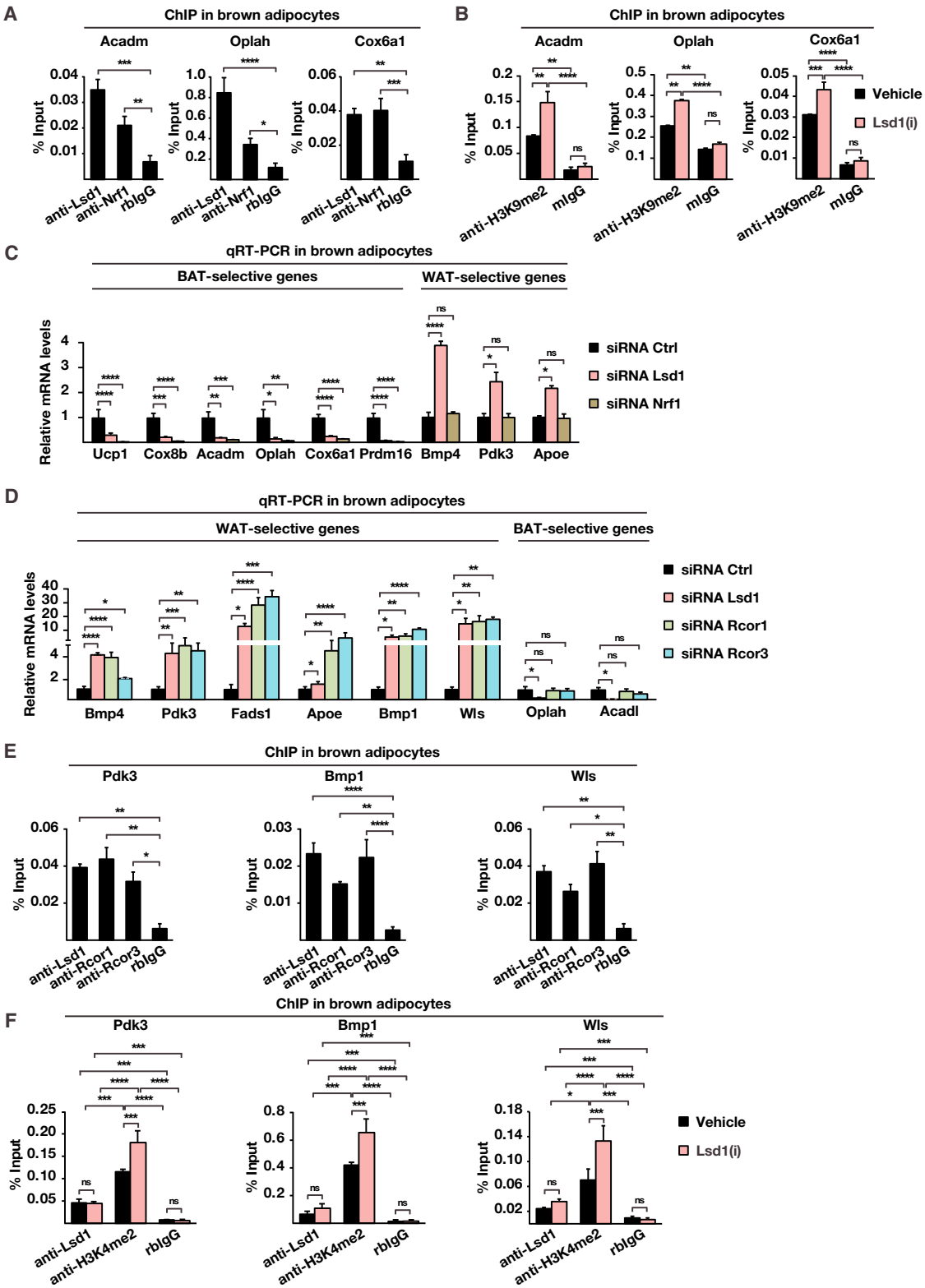

(legend on next page)

(Figure S3K). Because Lsd1 is known to repress gene expression by erasing dimethylation of lysine 4 of histone 3 (H3K4me2), we analyzed whether inhibition of Lsd1 is sufficient to alter methylation levels of H3K4 at WAT-selective genes. ChIP-qPCR analysis showed that levels of H3K4me2 were increased upon Lsd1(i) treatment at promoters of WAT-selective genes (Figure 3F). Concomitantly, levels of H3K9me2 were decreased at these promoters (Figure S3L), indicating an active transcriptional context. Together, our data demonstrate that Lsd1 represses WAT-selective gene expression in cooperation with the CoREST complex in BAT by reciprocal modulation of H3K4 and H3K9 methylation levels.

Loss of Lsd1 Induces Glycolysis while Repressing Oxidative Metabolism in BAT

Lsd1^{cKO} mice exhibit a profound morphological whitening of BAT associated with large lipid accumulation. To identify further changes in global gene expression in Lsd1^{cKO} mice that might account for the observed whitening of Lsd1-depleted brown fat, we performed a pathway enrichment analysis of the transcriptome data. The analysis (Figure 4A) uncovered pathways regulating energy production and fatty acid catabolism such as the tricarboxylic acid (TCA) cycle, electron transport chain (ETC), and β-oxidation. The expression of genes representing these pathways was downregulated (Figure 4B; Figure S4A), suggesting that oxidative metabolism is lowered in BAT of Lsd1^{cKO} mice, confirming our data in WAT (Duteil et al., 2014). Interestingly, the second most enriched pathway was "glycolysis and gluconeogenesis," which we did not observe in WAT. In line with these findings, we observed increased expression of glucose transporters and the majority of glycolytic enzymes catalyzing glucose-to-pyruvate conversion in Lsd1^{cKO} mice (Figure 4B; Figure S4B). We thus hypothesized that Lsd1 deficiency in BAT not only leads to reduction of oxidative functions but also increases glycolytic capacities. To evaluate bioenergetic changes upon inhibition of Lsd1, we employed a Seahorse XF analyzer (Agilent Technologies) to measure the extracellular acidification rate (ECAR) as an index of glycolytic activity (using a glycolysis stress kit) and the oxygen consumption rate (OCR) as an index of respiratory capacity (using the Cell Mito stress test kit) in brown adipocytes treated with Lsd1(i) or vehicle. The rate of glycolysis following glucose administration was higher upon Lsd1(i) treatment compared with vehicle (Figure 4C; Figure S4C). After addition of oligomycin, an inhibitor of mitochondrial ATP synthesis, the maximum glycolytic capacity of Lsd1(i)-treated cells remained higher than in control cells, demonstrating that not only the rate of glycolysis but also the glycolytic reserve capacity were enhanced in Lsd1-inactivated cells (Figure 4C; Figure S4C). In parallel, the OCR was lower in Lsd(i)-treated cells compared with vehicle (Figures S4D and S4E), and, subsequently, the OCR/ECAR ratio was decreased, demonstrating that Lsd1 inhibition shifted mitochondrial metabolism toward the glycolytic pathway in brown adipocytes (Figure 4D). Furthermore, oxygen consumption resulting from mitochondrial respiration measured in BAT of Lsd1^{cKO} mice was reduced compared with control mice, confirming lower oxidative phosphorylation (Figure S4F). Taken together, our data show that glycolytic activity is enhanced in the absence of Lsd1, whereas oxidative phosphorylation is reduced.

In addition, glucose uptake and activity of key glycolytic enzymes such as hexokinase (Hk), phosphofructokinase (Pfk), enolase (Eno), and lactate dehydrogenase (Ldh) were higher in BAT of Lsd1^{cKO} mice compared with control mice (Figure 4E), promoting increased glycolytic capacity.

Of note, the expression levels of genes involved in pyruvate metabolism, including the rate-limiting mitochondrial pyruvate transporters (Mpc1 and Mpc2) and enzymes catalyzing the conversion from pyruvate to acetyl-coenzyme A (CoA) (e.g., Dlat and Pdhx), were decreased in Lsd1^{cKO} mice (Figure 4B; Figure S4G). Our genome-wide analysis also revealed that expression of glutamic-oxaloacetic transaminase 1 (Got1) and 2 (Got2) as well as Slc25a12 and phosphoenolpyruvate carboxykinase 2 (Pck2) was upregulated in Lsd1^{cKO} mice compared with control (Figure 4B; Figure S4G). Got1 and 2 are responsible for conversion of downstream pyruvate intermediate oxaloacetate into aspartate and phosphoenolpyruvate, respectively (Birsoy et al., 2015). In particular, Got1 was shown to be essential for aspartate regeneration to restore ETC dysfunction (Birsoy et al., 2015). ETC dysfunction is associated with a drop in nicotinamide adenine dinucleotide (NAD^+)/NADH ratio because NAD^+ cannot be oxidized by complex I. However, despite decreased oxidative phosphorylation (OXPHOS), the NAD^+/NADH ratio was increased in BAT of Lsd1^{cKO} mice (Figure S4H). This might be, at least in part, mediated by higher Got1 activity (Figure 4E). An Increased NAD^+/NADH ratio is also in favor of increased glycolysis (Zhang et al., 2007).

Similarly, expression profiling of metabolic genes in Lsd1^{cKI} mice and mice treated with Lsd1(i) revealed that Lsd1 demethylase activity strongly contributes to maintaining proper energy metabolism in BAT (Figures S4B, S4G, and S4I). Taken together, these data show that glycolysis is enhanced in Lsd1-inactivated BAT, whereas oxidative metabolism is lowered.

The analysis of genome-wide Lsd1 chromatin occupancy in BAT by ChIP-seq revealed that glucose transporters and genes

Figure 3. Lsd1 Regulates the Brown Fat Program through a Dual Mechanism

(A and B) ChIP analysis to detect promoter occupancy performed with anti-Lsd1 and anti-Nrf1 antibodies or rabbit immunoglobulin G (IgG) (rbIgG) in wild-type brown adipocytes (A) and anti-H3K9me2 antibody or mouse IgG (mIgG) in brown adipocytes treated with Lsd1(i) or vehicle (B). The precipitated chromatin was quantified by qPCR analysis with primers flanking Lsd1-binding sites in the indicated genes.

(C and D) Relative mRNA levels of the indicated BAT- or WAT-selective genes in brown adipocytes transfected with unrelated control siRNA (siRNA Ctrl) or siRNA directed against Lsd1 (siRNA Lsd1) or Nrf1 (siRNA Nrf1) (C) and with siRNA Ctrl or siRNA directed against Rcor1 (siRNA Rcor1) or Rcor3 (siRNA Rcor3) (D).

(E and F) ChIP analysis to detect promoter occupancy performed with anti-Lsd1, anti-Rcor1, and anti-Rcor3 antibodies or rbIgG in brown adipocytes (E) and anti-Lsd1 and anti-H3K4me2 antibody or rbIgG in brown adipocytes treated with Lsd1(i) or vehicle (F). The precipitated chromatin was quantified by qPCR analysis with primers flanking Lsd1-binding sites in the indicated genes

Data are mean + SEM. (A), (C), (D), and (E): one-way ANOVA. (B) and (F): two-way ANOVA; *$p < 0.05$, **$p < 0.01$, ***$p < 0.001$, ****$p < 0.0001$; $n = 3$; qPCRs were run in triplicate. See also Figure S3 and Tables S2, S4, and S5.

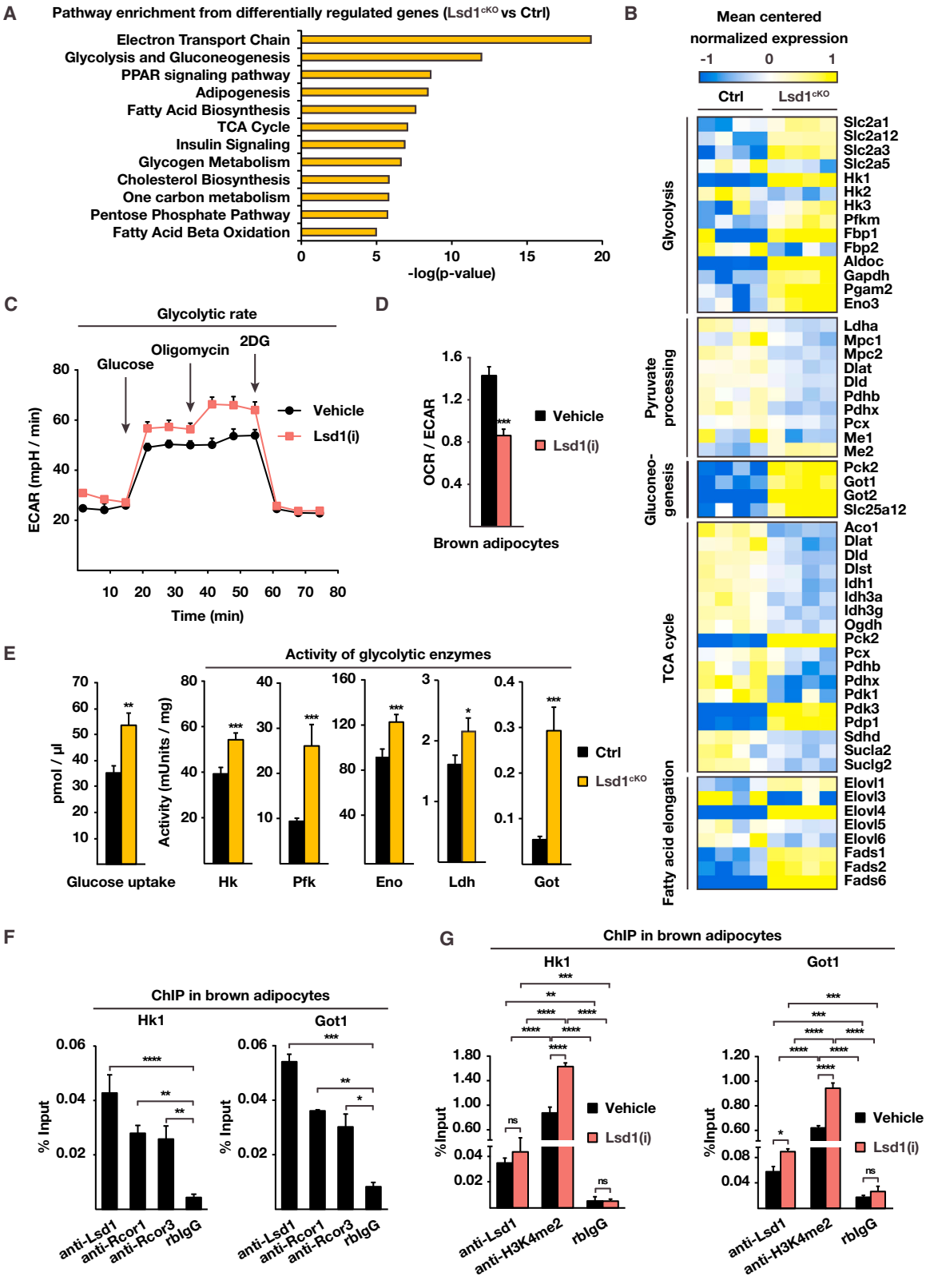

(legend on next page)

involved in glycolysis are direct targets of Lsd1 (Figure S4J). ChIP-qPCR of brown adipocytes showed promoter occupancy of representative genes by Rcor1, Rcor3, and Lsd1 (Figure 4F). In parallel, the levels of H3K4me2 were enriched, whereas the levels of H3K9me2 were lowered upon Lsd1(i) treatment (Figure 4G; Figures S4K and S4L). These results demonstrate that Lsd1 is directly repressing glycolytic genes to ensure physiological metabolic processes in brown adipocytes.

Lsd1 Regulates Lipid Accumulation in BAT

To further investigate our phenotype, we performed metabolomic and lipidomic analyses of BAT of 10-week-old control and $Lsd1^{cKO}$ mice. These analyses revealed an accumulation of intermediates of glycolysis, including glyceraldehyde-3-phosphate and glycerol, in BAT of $Lsd1^{cKO}$ mice (Figure 5A) accompanied by augmentation of long-chain diacyl- and triacylglycerides (DAGs and TAGs, respectively) (Figure 5B). In accordance with an increase in long-chain fatty acids, the transcript levels of fatty acid elongases (Elovl1, Elovl4, and Elovl7) and fatty acid desaturases (Fads1 and Fads2) were upregulated in the absence of Lsd1 (Figures 4B and 5C) or Lsd1 demethylase activity (Figures S5A and S5B). The analysis of genome-wide Lsd1 chromatin occupancy in BAT by ChIP-seq revealed that genes encoding enzymes involved in fatty acid elongation are direct targets of Lsd1 (Figures S5C–S5F).

DAG and TAG are glycerol esters derived from dihydroxyacetone phosphate (DHAP) and fatty acids. Allocation of fatty acids necessary for glyceride synthesis might be due to decreased lipolysis, increased de novo lipogenesis, or increased fatty acid uptake in BAT of $Lsd1^{cKO}$ mice. Increased fatty acid synthase (Fasn) activity (Figure 5D) and low acetyl-CoA carboxylase phosphorylation (Figure S5G) are in favor of enhanced de novo lipogenesis in $Lsd1^{cKO}$ mice. To assess lipolysis efficiency, we measured lipase activity. The activity of lipases present in brown adipocytes was reduced by 50% in $Lsd1^{cKO}$ mice, suggesting that hydrolysis of lipids into fatty acids is severely impaired (Figure 5E). In addition, the activity of lipoprotein lipase (Lpl), which hydrolyzes triglycerides in lipoproteins such as those found in chylomicrons and very low-density lipoprotein (VLDL) to facilitate fatty acid uptake from the bloodstream, was increased upon loss of Lsd1 (Figure 5F). Finally, to test whether fatty acid oxidation was altered, we measured mitochondrial respiration in the presence of palmitoyl-L-carnitine as substrate in saponine-permeabilized BAT. The data revealed that Lsd1-deficient BAT failed to properly use fatty acids (Figure 5G). Increased fatty acid synthesis and lower lipolysis are in agreement with the observation of an increased NAD^+/NADH ratio (Figure S4H). Altogether, these findings show that Lsd1 regulates lipid accumulation in BAT.

In summary, our data show that Lsd1 positively regulates the expression of oxidative metabolism-related genes with concomitant repression of the gene program responsible for glycolysis and fatty acid biosynthesis. Accordingly, loss of Lsd1 in brown adipose tissue drives a shift from oxidative to glycolytic metabolism accompanied by aberrant triglyceride accumulation.

Absence of Lsd1 Improves Glucose Uptake Despite Increasing Body Weight

Finally, we examined the consequences of Lsd1 loss in BAT with aging. $Lsd1^{cKO}$ male mice gained significantly more weight (~40%) than their control littermates between 10 and 30 weeks of age (Figure 6A). No weight differences were observed in females (Figure S6A). The weight gain of $Lsd1^{cKO}$ mice was not due to increased food intake or decreased mobility (Figures S6B–S6D). Body composition analysis assessed with a whole-body magnetic resonance analyzer (EchoMRI) revealed that 30-week-old $Lsd1^{cKO}$ mice accumulated more fat than their control littermates, resulting in a lower lean/fat mass ratio compared with control mice (Figure 6B). These data were corroborated by a dramatically increased BAT mass in 30-week-old $Lsd1^{cKO}$ mice as well as in $Lsd1^{cKI}$ mice (Figures S6E and S6F), associated with ~45% augmentation in fatty acid content of BAT (Figure 6C). In accordance, histological analyses revealed a robust phenotypic conversion of BAT in $Lsd1^{cKO}$ and $Lsd1^{cKI}$ mice to a WAT-like appearance (Figure S6G). In addition, we noticed robustly reduced Ucp1 protein levels, as shown by immunocytochemistry (Figure S6G). Observed morphological changes in BAT are accompanied by increased levels of intermediates of glycolysis, glycerol, DAG, and TAG (Figures S6H and S6I).

In 30-week-old $Lsd1^{cKO}$ mice, we observed lower energy expenditure, determined by decreased whole-body oxygen consumption (VO_2) (Figure 6D; Figures S6J and S6K) and CO_2 production (VCO_2) (Figure 6E; Figures S6L and S6M), resulting in an increased respiratory quotient (RQ, VCO_2/VO_2 ratio) (Figure 6F). This confirmed a shift in fuel consumption from fatty acids to carbohydrates. In addition, calorimetric parameters deduced from these analyses indicated that energy expenditure was decreased in $Lsd1^{cKO}$ mice (Figure 6G; Figures S6N and S6O). This was confirmed by body temperature measurements (Figure 6H).

Figure 4. Lsd1 Represses Glycolysis in BAT

(A) Enriched pathways obtained from gene ontology (GO) term analysis for genes differentially expressed in BAT of $Lsd1^{cKO}$ and control mice.

(B) Heatmaps depicting mean centered normalized mRNA expression of selected genes involved in the TCA cycle, fatty acid elongation, glycolysis, pyruvate processing, and gluconeogenesis in BAT of Ctrl and $Lsd1^{cKO}$ mice at 10 weeks of age (Ctrl, n = 4; $Lsd1^{cKO}$, n = 4).

(C and D) Representative ECAR (C) and OCR divided by ECAR (D) for Lsd1(i)- or vehicle-treated brown adipocytes determined with the Seahorse extracellular flux analyzer (mean + SEM, ***$p < 0.001$, n = 6).

(E) Determination of glucose uptake, Hk, Pfk, Eno, Ldh, and Got activities in BAT of Ctrl and $Lsd1^{cKO}$ mice at 10 weeks of age (mean + SEM, *$p < 0.05$, ***$p < 0.001$, n = 5).

(F and G) ChIP analysis to detect promoter occupancy performed with anti-Lsd1, anti-Rcor1, and anti-Rcor3 antibodies or rbIgG in brown adipocytes (F) and anti-Lsd1 and anti-H3K4me2 antibody or rbIgG in brown adipocytes (G) treated with vehicle or Lsd1(i). The precipitated chromatin was quantified by qPCR analysis with primers flanking Lsd1-binding sites in the indicated genes (mean + SEM). (F): one-way ANOVA. (G): two-way ANOVA. ns: $p > 0.05$, *$p < 0.05$, **$p < 0.01$, ***$p < 0.001$, ****$p < 0.0001$; n = 3; qPCRs were run in triplicate).

See also Figure S4.

A

Peak.ID	Compound_Name	Lsd1^{cKO} (mean+/-SEM)	Ctrl (mean+/-SEM)	fold change	f-test	t-test
GC_019	Glycerol	72.06+/- 9.32	29.44+/- 2.52	2.45	0.34	0.01
GC_020	Glycerol 3-phosphate	5.40+/- 0.36	6.85+/- 0.44	0.79	1.34	0.02
PN_296	Glyceraldehyde 3-phosphate	0.05+/- 0.02	0.01+/- 0.01	8.58	2.34	0.04
PN_325	N-Acetylaspartic acid	0.35+/- 0.05	0.64+/- 0.06	0.55	3.34	0.01
GC_008	Citric acid	2.60+/- 0.25	1.87+/- 0.21	1.39	4.34	0.04
GC_012	Fructose 6-phosphate	0.34+/- 0.08	0.10+/- 0.03	3.57	5.34	0.02
GC_016	Glucose 6-phosphate	2.09+/- 0.51	0.53+/- 0.23	3.93	6.34	0.02
GC_010	Cysteine	0.26+/- 0.03	0.20+/- 0.00	1.32	7.34	0.05
GC_036	Pyruvic acid	3.79+/- 0.97	1.74+/- 0.20	2.18	8.34	0.06
PN_398	N-Acetylglutamic acid	0.20+/- 0.06	0.10+/- 0.01	2.08	9.34	0.09
GC_038	Succinic acid	2.52+/- 0.26	1.69+/- 0.18	1.49	10.34	0.02
GC_014	Glucose	11.87+/- 1.39	8.17+/- 0.58	1.45	11.34	0.03
GC_017	Glutamic acid	6.21+/- 0.33	5.01+/- 0.32	1.24	12.34	0.02
GC_030	Malic acid	5.17+/- 0.78	3.33+/- 0.57	1.55	13.34	0.05
GC_006	Aspartic acid	4.69+/- 0.36	4.10+/- 0.15	1.14	14.34	0.10

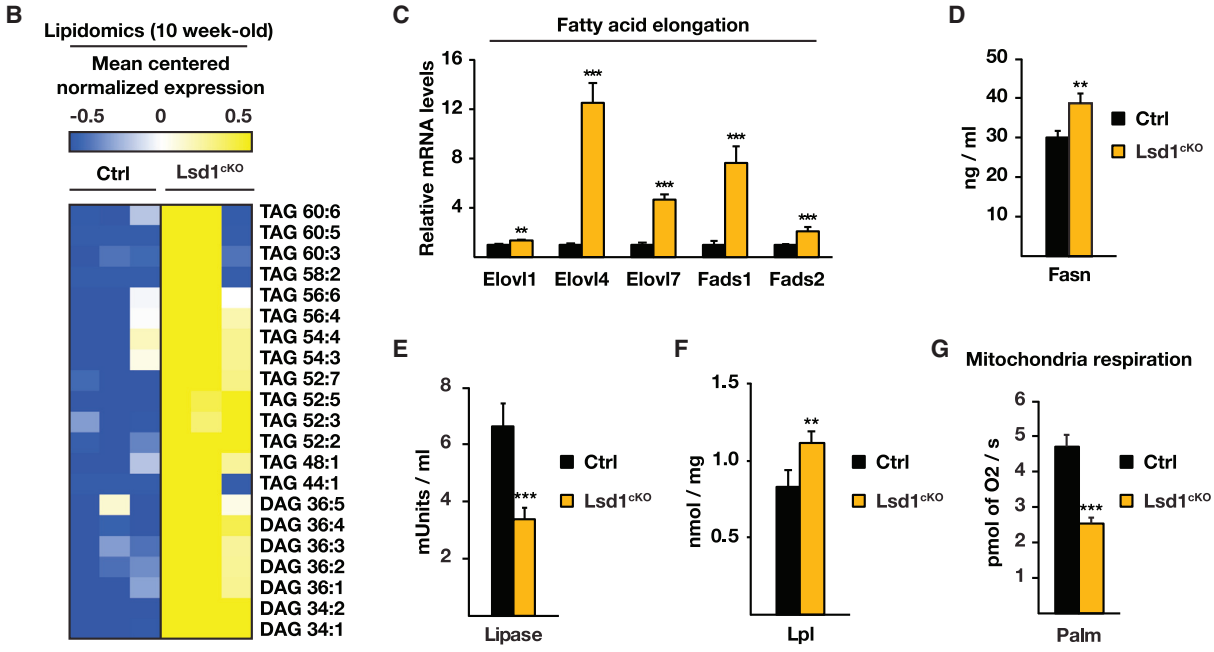

Figure 5. Lsd1 Limits Fat Accumulation in BAT

(A) Metabolomic analysis of BAT of control and Lsd1^{cKO} mice.

(B) Lipidomic analysis of BAT from 10-week-old control and Lsd1^{cKO} mice.

(C) Relative mRNA levels of the indicated enzymes involved in fatty acid elongation in BAT of control and Lsd1^{cKO} mice (mean + SEM; $^{**}p < 0.01$, $^{***}p < 0.001$; Ctrl, n = 9; Lsd1^{cKO}, n = 7).

(D–F) Determination of fatty acid synthase (Fasn), lipase, and Lpl activities in BAT of Ctrl and Lsd1^{cKO} mice at 10 weeks of age (mean + SEM, $^{**}p < 0.01$, $^{***}p < 0.001$, n = 6).

(G) Mitochondrial respiration of BAT extracts from Ctrl and Lsd1^{cKO} mice assessed with a high-resolution respiratory Oxygraph-2K system using palmitoyl-L-carnitine as substrate (mean + SEM, $^{***}p < 0.001$, n = 6).

See also Figure S5 and Tables S4 and S5.

Next we analyzed mice for glucose tolerance and insulin sensitivity. We observed that circulating glucose levels in 10-week-old Lsd1^{cKO} mice were lower compared with control littermates (Figure 6I). Nevertheless, we did not notice any difference in glucose tolerance of Lsd1^{cKO} mice relative to control mice at this age (Figure 6J). Importantly, with aging, control mice developed progressive glucose intolerance, contrary to Lsd1^{cKO} mice, which conserved efficient glucose uptake (Figure 6J). Age-developed glucose intolerance is generally associated with loss of insulin sensitivity and contributes to type 2 diabetes. To unravel whether Lsd1^{cKO} mice are resistant to age-induced type 2 diabetes, we performed an intraperitoneal insulin sensitivity test (IPIST) and determined serum insulin levels. Despite dramatic alterations in glucose metabolism, we did not observe any difference in insulin

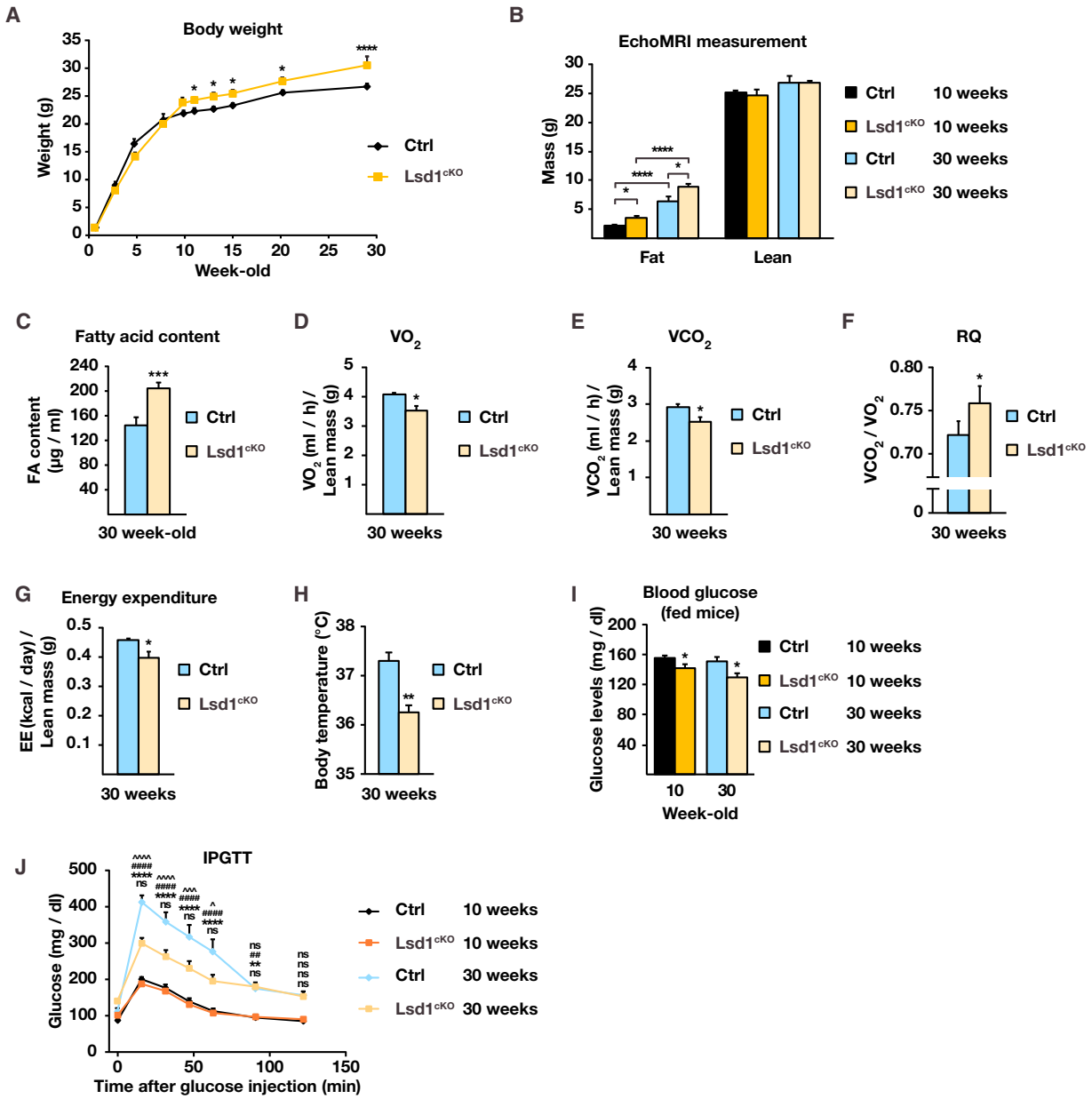

Figure 6. Lsd1^{cKO} Mice Have Higher Glucose Uptake Despite Increased Body Weight

(A) Body weight of control and Lsd1^{cKO} mice at the indicated age (mean + SEM; two-way ANOVA with repeated measures; factor interaction, $p_{genotype/time}$ < 0.0001; *p < 0.05, ***p < 0.001; n = 7).

(B and C) Body fat and lean content(B) and fatty acid content (C) of 30-week-old control and Lsd1^{cKO} mice. (B) and (C): mean + SEM, *p < 0.05, ***p < 0.001, ****p < 0.0001. (B): two-way ANOVA, n = 7. (C): n = 5.

(D–G) VO_2 (D), VCO_2 (E), RQ (F), and energy expenditure (G) of 30-week-old control and Lsd1^{cKO} mice (mean + SEM; *p < 0.05, **p < 0.01; Ctrl, n = 8; Lsd1^{cKO}, n = 7). VO_2, VCO_2, and energy expenditure are normalized to the lean mass.

(H) Body temperature of 30-week-old control and Lsd1^{cKO} mice (mean + SEM; **p < 0.01; Ctrl, n = 8; Lsd1^{cKO}, n = 7).

(I) Serum glucose levels of fed Ctrl and Lsd1^{cKO} mice at the indicated ages (mean + SEM; *p < 0.05; Ctrl, n = 8; Lsd1^{cKO}, n = 7).

(J) Intraperitoneal glucose tolerance test (IPGTT) for 10-week-old or 30-week-old control and Lsd1^{cKO} mice starved for 6 hr prior to analysis (mean + SEM; two-way ANOVA; Ctrl 10-week-old versus Lsd1^{cKO} 10-week-old, ns p > 0.05; Ctrl 10-week-old versus Ctrl 30-week-old, **p < 0.01, ****p < 0.0001; Lsd1^{cKO} 10-week-old versus Lsd1^{cKO} 30-week-old, ##p < 0.01, ####p < 0.0001; Ctrl 30-week-old versus Lsd1^{cKO} 30-week-old, ns p > 0.05, ^p < 0.05, ^^^p < 0.001, ^^^^p < 0.0001; Ctrl, n = 8; Lsd1^{cKO}, n = 7).

See also Figure S6.

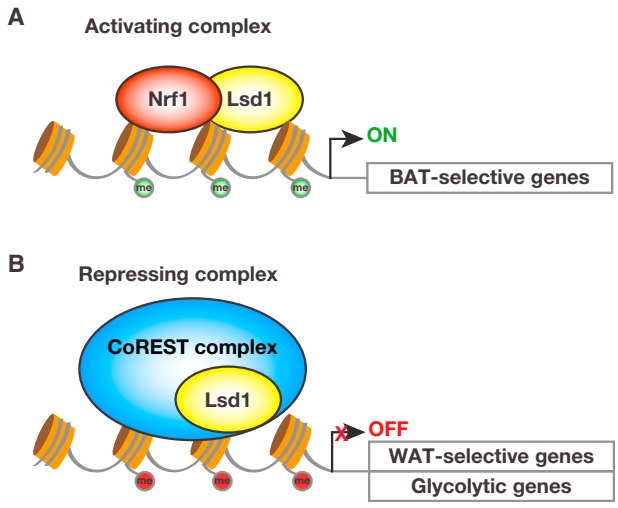

Figure 7. Lsd1 Governs the Gene Expression Program and Metabolic Functions of Brown Adipose Tissue

Lsd1 controls the properties of BAT via a dual mechanism, resulting in inhibition of WAT-selective and promotion of BAT-selective gene expression. This opposing function of Lsd1 is orchestrated via interaction with (A) the activating transcription factor Nrf1 (H3K4me2 marks are depicted in green) and (B) an Lsd1-containing repressive CoREST complex (H3K9me2 marks are depicted in red).

sensitivity (Figure S6P) or in total insulin levels (Figure S6Q), showing that only glucose but not insulin metabolism is altered in Lsd1^{cKO} mice. In summary, these data show that Lsd1 is required in BAT to maintain a proper energy balance with aging.

DISCUSSION

White and brown adipocytes have distinct transcriptional programs that facilitate long-term lipid storage or thermogenesis, respectively. Understanding these programs is of the highest interest for developing new strategies to counteract obesity. The epigenetic determinants that regulate white versus brown fat-selective gene expression have not yet been completely elucidated. In this study, we show that the histone demethylase Lsd1 plays a key role in the maintenance of brown fat metabolic properties. Lsd1 accomplishes this mission via a dual mechanism by inhibiting the expression of WAT-selective genes and simultaneously promoting the expression of BAT-selective genes. These opposing functions of Lsd1 are orchestrated by the assembly in different protein complexes: a repressive CoREST complex to inhibit the expression of WAT-selective genes and an Nrf1-containing complex to promote the expression of BAT-selective genes (Figure 7). Our data point out the importance of Lsd1 demethylase activity in controlling BAT metabolism in vivo. Indeed, our engineered mouse model, Lsd1^{cKI} mice, as well as wild-type mice treated with an Lsd1-specific inhibitor, basically recapitulate the phenotype observed in Lsd1^{cKO} mice. Alterations in BAT morphology and transcriptome in Lsd1^{cKI} and Lsd(i)-treated mice resemble that of Lsd1^{cKO} mice and suggest that catalytically active Lsd1 significantly contributes to the maintenance of the BAT gene expression program and function. However, additional scaffolding functions of Lsd1, which might be independent of the enzymatic activity (i.e., the recruitment of proteins and/or the assembly in different protein complexes) might be impaired upon loss of Lsd1 in Lsd1^{cKO} mice. In contrast, in knockin mice, the enzymatically inactive Lsd1 mutant protein might be able to perform, at least in part, these functions, which might explain a less severe phenotype.

Lsd1 exerts its function in brown adipocytes by engaging in different protein complexes. Coordinated action of Lsd1 with members of the CoREST complex, in particular Rcor1 and Rcor3, represses the expression of WAT-selective genes. Although Lsd1 has been shown to interact with CoREST in various tissues (Lee et al., 2005; Metzger et al., 2005; Shi et al., 2004; Yang et al., 2011), the physiological function of CoREST in vivo remains unclear. Here we demonstrate for the time that the CoREST complex plays a critical role in the repression of the WAT-selective genes in BAT, thereby strongly contributing to the maintenance of brown fat characteristics. In BAT, Lsd1 specifically associates with Rcor1 and Rcor3 but not Rcor2. Similar to Lsd1, Rcor1 is ubiquitously expressed in somatic cells, whereas the expression of Rcor2 and Rcor3 seems to be more restricted (Yang et al., 2011). This suggests that the Lsd1 corepressor complex might assemble with different Rcor family members to carry out specific functions in different cell types.

Furthermore, Lsd1 interacts with Nrf1 to activate the expression of BAT-selective genes. We have shown previously that, in WAT, Lsd1 acts together with Nrf1 to positively regulate OXPHOS and thermogenesis (Duteil et al., 2014). Elevated Lsd1 levels favor beigening of WAT by increasing oxidative metabolism, uncoupling, thermogenesis, and the number and size of mitochondria. Our data provide evidence that the absence of Lsd1 in BAT causes dramatic mitochondrial dysfunction associated with decreased transcript levels of OXPHOS-related genes. It is interesting that Lsd1 in cooperation with Nrf1 shares comparable functions in beige and brown adipocytes. Whether the mechanism of regulation of oxidative metabolism is conserved in all metabolically active tissues remains unclear. To clarify this hypothesis, it would be necessary to analyze the metabolism of skeletal muscle and liver in Lsd1 knockout mice.

Our analyses uncovered that Lsd1 is necessary to regulate metabolism, particularly fatty acid oxidation, de novo lipogenesis, and lipolysis, leading to increased DAG and TAG accumulation and whitening of Lsd1^{cKO} BAT. In addition, Lsd1 depletion/inhibition leads to elevated glucose uptake and increased glycolytic capacities in mice. This may contribute to DAG and TAG accumulation because the glycerol backbone for triglyceride synthesis can be derived from the glycolytic intermediate dihydroxyacetone phosphate. Furthermore, pyruvate is converted into citrate in the TCA cycle and utilized to provide acetyl-CoA to initiate de novo lipogenesis. However, further experiments would be necessary to provide a direct link between these processes. Nevertheless, the role of Lsd1 in lipid metabolism has been confirmed in this study because Lsd1^{cKO} mice show increased activity of fatty acid synthase and decreased activity of lipases. Altogether, alterations in glycolysis and fatty acid oxidation might contribute to aberrant production of DAG and TAG, which leads to increased fat accumulation.

Transcriptional and metabolic changes induced by Lsd1 ablation have secondary effects on body weight gain and glucose tolerance with aging. Indeed, Lsd1^{cKO} mice gained significantly more weight than their control littermates. These findings are of interest, considering that many mouse models possessing defects in adipose tissue function and metabolism, such as loss of mitochondrial uncoupling (Liu et al., 2003) and fatty acid or ceramide metabolism (Ellis et al., 2010; Lee et al., 2016; Schoiswohl et al., 2015; Turpin et al., 2014), do not develop obesity. A hypothesis might be that Lsd1-deficient brown adipocytes secrete signaling molecules that exert a potential inhibitory function on energy expenditure in other metabolic organs such as white adipose tissue, liver, or muscle. Consequently, we carefully inspected our transcriptome analysis for differential expression of endocrine molecules, cytokines, or other signaling molecules. This analysis failed to identify any known candidates that might explain the phenotype in our mice. This, however, does not exclude the possibility that Lsd1 regulates the expression of yet undescribed endocrine molecules in brown adipocytes. Future studies will be required to elucidate this issue.

Previous studies showed that the ablation of the brown fat-determining transcriptional regulator Prdm16 is required to suppress the expression of WAT-selective genes in BAT (Harms et al., 2014) similar to Lsd1. However, the expression of the most typical BAT-selective genes was only slightly reduced upon *Prdm16* ablation, which could explain why Prdm16 knockout mice are not prone to obesity (Harms et al., 2014). In line with this publication, Zeng et al. (2016) showed that Lsd1 associates with Prdm16 to repress expression of WAT-selective genes. Of note, our ChIP-seq data identified *Prdm16* as a direct Lsd1 target, and *Prdm16* expression was reduced in Lsd1-deleted BAT. However, immunoprecipitation, size exclusion chromatography, and mass spectrometry analyses did not provide any evidence for association of Lsd1 and Prdm16 in BAT, suggesting that Lsd1 acts upstream of Prdm16. Zeng et al. (2016) also claim that Lsd1 represses the expression of hydroxysteroid 11-β-dehydrogenase isozyme 1 (*Hsd11b1*) independently from Prdm16. Even though *Hsd11b1* is 1.5-fold upregulated in our Lsd1^{cKO} mice, our cistrome analysis did not provide any evidence for binding of Lsd1 to the Hsd11b1 promoter. Even though the phenotypes of our Lsd1^{cKO} mice and the mice engineered by Zeng et al. (2016) are close, the differences observed in the follow-up cistrome and transcriptome analyses and the interpretation of the molecular mechanism could be explained by the fact that they did not use a brown fat-specific Cre deleter strain.

Recently, Sambeat et al. (2016) proposed that Zfp516 associates with Lsd1 to promote Ucp1 promoter occupancy and gene expression. In clear contrast, our mass spectrometry analysis does not confirm interaction of endogenously expressed Lsd1 and Zfp516 in brown adipocytes. In addition, our ChIP-seq showed that the Ucp1 promoter is not occupied by Lsd1 in brown adipocytes.

Our findings indicate that the use of Lsd1 inhibitors would lead to a shift from oxidative to glycolytic metabolism in BAT, resulting in weight gain but improved glucose tolerance. These findings need to be considered because Lsd1 inhibitors entered clinical trials, for example in the treatment of mixed-lineage leukemia (Feng et al., 2016). In conclusion, our data identify Lsd1 as a key epigenetic regulator of BAT metabolism.

EXPERIMENTAL PROCEDURES

Mouse Studies

All mice were housed in the pathogen-free barrier facility of the University Medical Center Freiburg in accordance with institutional guidelines approved by the regional board. Mice were maintained in a temperature- and humidity-controlled animal facility with a 12-hr light/dark cycle, free access to water, and a standard rodent chow (Kliba, breeding, 3807). Male mice were analyzed at 10 or 30 weeks of age. Animals were killed by cervical dislocation, and tissues were immediately collected, weighed, frozen in liquid nitrogen, or processed for further analyses. In vivo experiments, including food consumption, serum analysis, glucose tolerance tests, temperature measurements, and energy expenditure, were described previously (Duteil et al., 2014). The Lsd1 inhibitor QC6688 was administrated per os at 5 mg/kg in 0.5% methylcellulose (Sigma; product M0512-110G; viscosity, 4,000 centipoise [cP]).

Cellular Metabolism

Cellular metabolic rates were measured using an XF24 analyzer (Seahorse Bioscience). Immediately before the measurement, cells were washed with unbuffered DMEM as described previously (Wu et al., 2007). Plates were placed into the XF24 instrument for measurement of OCR and ECAR with the XFp glycolysis stress kit (103017-100, Seahorse) for ECAR measurements (glucose, 10 mM; oligomycin, 1 μM; and 2 deoxiglucose (2-DG), 50 mM) or the Cell Mito stress kit (103010-100, Seahorse) for OCR measurements (oligomycin, 1 μM; carbonyl cyanide-4-(trifluoromethoxy)phenylhydrazone (FCCP), 0.5 μM; and rotenone/antimycin A, 0.25 μM).

Lipid Quantification

Total lipids were extracted from 50 mg of BAT using a lipid extraction kit (STA-612, Cell Biolabs) and quantified using a lipid quantification kit (STA-613, Cell Biolabs) according to the manufacturer's recommendations.

Quantification of Mitochondrial and Nuclear DNA

BAT was digested overnight with Proteinase K, and DNA was extracted with phenol-chloroform. Mitochondria and nuclear DNA were amplified by qPCR using *Cox2* and *Fasn* primers (Table S4), respectively.

Metabolomic and Lipidomic Analyses

Tissue samples were grinded with a Retsch MM440 instrument and further extracted as described in Giavalisco et al. (2009). LC-MS measurements were performed using a Waters ACQUITY ultra performance liquid chromatography (UPLC) system coupled to a Thermo Fisher Scientific QExactive mass spectrometer. Details of the analysis are presented in the Supplemental Experimental Procedures.

Data Analysis

Data are represented as mean + SEM. Significance was calculated by

(1) two-tailed Student's t test for Figures 1G and 1H, 2C and 2D, 4D and 4E, 5C–5G, and 6C–6I and Figures S1A, S1D, S2A, S2C, S2D, S4B, S4C, S4E–S4I, S5A, S5B, S6B–S6E, S6J, S6L, S6N, and S6Q;
(2) one-way ANOVA for Figures 3A and 3C–3E and 4F and Figures S3A, S3E, S3K, and S5D;
(3) two-way ANOVA for Figures 3B and 3F, 4G, and 6A, 6B, and 6J and Figures S3B, S3L, S4K, S4L, S5E, S5F, S6A, and S6P;
(4) Wilcoxon rank-sum test for Figures 5A and 5B and Figures S6H and S6I; and
(5) analysis of covariance (ANCOVA) for Figures S6K, S6M, and S6O.

Heatmaps were generated by centering and normalizing expression values with Cluster 3.0 and importing them to MeV viewer.

ACCESSION NUMBERS

The accession numbers for the RNA-seq and ChIP-seq data reported in this paper are GEO: GSE81557 and GEO: GSE81557, respectively. The accession number for the mass spectrometry proteomics data reported in this paper is ProteomeXchange Consortium/PRIDE (Vizcaíno et al., 2016) partner repository: PXD004745.

SUPPLEMENTAL INFORMATION

Supplemental Information includes Supplemental Experimental Procedures, seven figures, and five tables and can be found with this article online at http://dx.doi.org/10.1016/j.celrep.2016.09.053.

AUTHOR CONTRIBUTIONS

R.S. generated the original hypothesis. D.D., M.T., J.M.M., S.U., F.L., T.K., and H.Z.N. performed the experiments. L.A. and T.M. performed the ChIP-seq analysis. D.W. and D.D. performed the bioinformatics analyses. K.P. and J.D. performed the mass spectrometry analysis. N.M. performed the electron microscopy analysis. V.Z. and M.M. performed the lipidomic and metabolomics analyses. J.W.K. and J.C.B. provided the Ucp1-Cre mice. D.D. and R.S. took primary responsibility for writing the manuscript. All authors edited the manuscript.

ACKNOWLEDGMENTS

We are obliged to F. Pfefferle and L. Walz for providing excellent technical assistance and T. Günther, H. Greschik, and M.J. Castex Armendariz for helpful discussions. This work was supported by grants from the European Research Council (ERC AdGrant 322844 to R.S.) and Deutsche Forschungsgemeinschaft (SFB 992, 850, 746, and Schu688/12-1 to R.S.).

Received: July 22, 2016
Revised: September 6, 2016
Accepted: September 15, 2016
Published: October 18, 2016

REFERENCES

Betz, M.J., and Enerbäck, S. (2015). Human Brown Adipose Tissue: What We Have Learned So Far. Diabetes *64*, 2352–2360.

Birsoy, K., Wang, T., Chen, W.W., Freinkman, E., Abu-Remaileh, M., and Sabatini, D.M. (2015). An Essential Role of the Mitochondrial Electron Transport Chain in Cell Proliferation Is to Enable Aspartate Synthesis. Cell *162*, 540–551.

Cai, C., He, H.H., Gao, S., Chen, S., Yu, Z., Gao, Y., Chen, S., Chen, M.W., Zhang, J., Ahmed, M., et al. (2014). Lysine-specific demethylase 1 has dual functions as a major regulator of androgen receptor transcriptional activity. Cell Rep. *9*, 1618–1627.

Cannon, B., and Nedergaard, J. (2004). Brown adipose tissue: function and physiological significance. Physiol. Rev. *84*, 277–359.

Cohen, P., and Spiegelman, B.M. (2015). Brown and Beige Fat: Molecular Parts of a Thermogenic Machine. Diabetes *64*, 2346–2351.

Duteil, D., Metzger, E., Willmann, D., Karagianni, P., Friedrichs, N., Greschik, H., Günther, T., Buettner, R., Talianidis, I., Metzger, D., and Schüle, R. (2014). LSD1 promotes oxidative metabolism of white adipose tissue. Nat. Commun. *5*, 4093.

Ellis, J.M., Li, L.O., Wu, P.C., Koves, T.R., Ilkayeva, O., Stevens, R.D., Watkins, S.M., Muoio, D.M., and Coleman, R.A. (2010). Adipose acyl-CoA synthetase-1 directs fatty acids toward beta-oxidation and is required for cold thermogenesis. Cell Metab. *12*, 53–64.

Feng, Z., Yao, Y., Zhou, C., Chen, F., Wu, F., Wei, L., Liu, W., Dong, S., Redell, M., Mo, Q., and Song, Y. (2016). Pharmacological inhibition of LSD1 for the treatment of MLL-rearranged leukemia. J. Hematol. Oncol. *9*, 24.

Fitzgibbons, T.P., Kogan, S., Aouadi, M., Hendricks, G.M., Straubhaar, J., and Czech, M.P. (2011). Similarity of mouse perivascular and brown adipose tissues and their resistance to diet-induced inflammation. Am. J. Physiol. Heart Circ. Physiol. *301*, H1425–H1437.

Giavalisco, P., Köhl, K., Hummel, J., Seiwert, B., and Willmitzer, L. (2009). 13C isotope-labeled metabolomes allowing for improved compound annotation and relative quantification in liquid chromatography-mass spectrometry-based metabolomic research. Anal. Chem. *81*, 6546–6551.

Giralt, M., Martin, I., Iglesias, R., Viñas, O., Villarroya, F., and Mampel, T. (1990). Ontogeny and perinatal modulation of gene expression in rat brown adipose tissue. Unaltered iodothyronine 5′-deiodinase activity is necessary for the response to environmental temperature at birth. Eur. J. Biochem. *193*, 297–302.

Harms, M.J., Ishibashi, J., Wang, W., Lim, H.W., Goyama, S., Sato, T., Kurokawa, M., Won, K.J., and Seale, P. (2014). Prdm16 is required for the maintenance of brown adipocyte identity and function in adult mice. Cell Metab. *19*, 593–604.

Kleiner, S., Mepani, R.J., Laznik, D., Ye, L., Jurczak, M.J., Jornayvaz, F.R., Estall, J.L., Chatterjee Bhowmick, D., Shulman, G.I., and Spiegelman, B.M. (2012). Development of insulin resistance in mice lacking PGC-1α in adipose tissues. Proc. Natl. Acad. Sci. USA *109*, 9635–9640.

Langin, D. (2010). Recruitment of brown fat and conversion of white into brown adipocytes: strategies to fight the metabolic complications of obesity? Biochim. Biophys. Acta *1801*, 372–376.

Lee, M.G., Wynder, C., Cooch, N., and Shiekhattar, R. (2005). An essential role for CoREST in nucleosomal histone 3 lysine 4 demethylation. Nature *437*, 432–435.

Lee, Y.H., Jung, Y.S., and Choi, D. (2014a). Recent advance in brown adipose physiology and its therapeutic potential. Exp. Mol. Med. *46*, e78.

Lee, Y.H., Mottillo, E.P., and Granneman, J.G. (2014b). Adipose tissue plasticity from WAT to BAT and in between. Biochim. Biophys. Acta *1842*, 358–369.

Lee, J., Choi, J., Aja, S., Scafidi, S., and Wolfgang, M.J. (2016). Loss of Adipose Fatty Acid Oxidation Does Not Potentiate Obesity at Thermoneutrality. Cell Rep. *14*, 1308–1316.

Liu, X., Rossmeisl, M., McClaine, J., Riachi, M., Harper, M.E., and Kozak, L.P. (2003). Paradoxical resistance to diet-induced obesity in UCP1-deficient mice. J. Clin. Invest. *111*, 399–407.

Metzger, E., Wissmann, M., Yin, N., Müller, J.M., Schneider, R., Peters, A.H., Günther, T., Buettner, R., and Schüle, R. (2005). LSD1 demethylates repressive histone marks to promote androgen-receptor-dependent transcription. Nature *437*, 436–439.

Metzger, E., Willmann, D., McMillan, J., Forne, I., Metzger, P., Gerhardt, S., Petroll, K., von Maessenhausen, A., Urban, S., Schott, A.K., et al. (2016). Assembly of methylated KDM1A and CHD1 drives androgen receptor-dependent transcription and translocation. Nat. Struct. Mol. Biol. *23*, 132–139.

Musri, M.M., Carmona, M.C., Hanzu, F.A., Kaliman, P., Gomis, R., and Párrizas, M. (2010). Histone demethylase LSD1 regulates adipogenesis. J. Biol. Chem. *285*, 30034–30041.

Peirce, V., and Vidal-Puig, A. (2013). Regulation of glucose homoeostasis by brown adipose tissue. Lancet Diabetes Endocrinol. *1*, 353–360.

Puigserver, P., Wu, Z., Park, C.W., Graves, R., Wright, M., and Spiegelman, B.M. (1998). A cold-inducible coactivator of nuclear receptors linked to adaptive thermogenesis. Cell *92*, 829–839.

Sambeat, A., Gulyaeva, O., Dempersmier, J., Tharp, K.M., Stahl, A., Paul, S.M., and Sul, H.S. (2016). LSD1 Interacts with Zfp516 to Promote UCP1 Transcription and Brown Fat Program. Cell Rep. *15*, 2536–2549.

Schoiswohl, G., Stefanovic-Racic, M., Menke, M.N., Wills, R.C., Surlow, B.A., Basantani, M.K., Sitnick, M.T., Cai, L., Yazbeck, C.F., Stolz, D.B., et al. (2015). Impact of Reduced ATGL-Mediated Adipocyte Lipolysis on Obesity-Associated Insulin Resistance and Inflammation in Male Mice. Endocrinology *156*, 3610–3624.

Shi, Y., Lan, F., Matson, C., Mulligan, P., Whetstine, J.R., Cole, P.A., Casero, R.A., and Shi, Y. (2004). Histone demethylation mediated by the nuclear amine oxidase homolog LSD1. Cell *119*, 941–953.

Tiraby, C., and Langin, D. (2003). Conversion from white to brown adipocytes: a strategy for the control of fat mass? Trends Endocrinol. Metab. *14*, 439–441.

Turpin, S.M., Nicholls, H.T., Willmes, D.M., Mourier, A., Brodesser, S., Wunderlich, C.M., Mauer, J., Xu, E., Hammerschmidt, P., Brönneke, H.S., et al. (2014). Obesity-induced CerS6-dependent C16:0 ceramide production promotes weight gain and glucose intolerance. Cell Metab. *20*, 678–686.

Vernochet, C., Mourier, A., Bezy, O., Macotela, Y., Boucher, J., Rardin, M.J., An, D., Lee, K.Y., Ilkayeva, O.R., Zingaretti, C.M., et al. (2012). Adipose-specific deletion of TFAM increases mitochondrial oxidation and protects mice against obesity and insulin resistance. Cell Metab. *16*, 765–776.

Vizcaíno, J.A., Csordas, A., del-Toro, N., Dianes, J.A., Griss, J., Lavidas, I., Mayer, G., Perez-Riverol, Y., Reisinger, F., Ternent, T., et al. (2016). 2016 update of the PRIDE database and its related tools. Nucleic Acids Res. *44* (*D1*), D447–D456.

Wu, M., Neilson, A., Swift, A.L., Moran, R., Tamagnine, J., Parslow, D., Armistead, S., Lemire, K., Orrell, J., Teich, J., et al. (2007). Multiparameter metabolic analysis reveals a close link between attenuated mitochondrial bioenergetic function and enhanced glycolysis dependency in human tumor cells. Am. J. Physiol. Cell Physiol. *292*, C125–C136.

Wu, J., Boström, P., Sparks, L.M., Ye, L., Choi, J.H., Giang, A.H., Khandekar, M., Virtanen, K.A., Nuutila, P., Schaart, G., et al. (2012). Beige adipocytes are a distinct type of thermogenic fat cell in mouse and human. Cell *150*, 366–376.

Yang, P., Wang, Y., Chen, J., Li, H., Kang, L., Zhang, Y., Chen, S., Zhu, B., and Gao, S. (2011). RCOR2 is a subunit of the LSD1 complex that regulates ESC property and substitutes for SOX2 in reprogramming somatic cells to pluripotency. Stem Cells *29*, 791–801.

Zeng, X., Jedrychowski, M.P., Chen, Y., Serag, S., Lavery, G.G., Gygi, S.P., and Spiegelman, B.M. (2016). Lysine-specific demethylase 1 promotes brown adipose tissue thermogenesis via repressing glucocorticoid activation. Genes Dev. *30*, 1822–1836.

Zhang, Q., Wang, S.Y., Fleuriel, C., Leprince, D., Rocheleau, J.V., Piston, D.W., and Goodman, R.H. (2007). Metabolic regulation of SIRT1 transcription via a HIC1:CtBP corepressor complex. Proc Natl Acad Sci USA *104*, 829–833.

Zhu, D., Hölz, S., Metzger, E., Pavlovic, M., Jandausch, A., Jilg, C., Galgoczy, P., Herz, C., Moser, M., Metzger, D., et al. (2014). Lysine-specific demethylase 1 regulates differentiation onset and migration of trophoblast stem cells. Nat. Commun. *5*, 3174.

Cell Reports, Volume *17*

Supplemental Information

Lsd1 Ablation Triggers Metabolic Reprogramming of Brown Adipose Tissue

Delphine Duteil, Milica Tosic, Franziska Lausecker, Hatice Z. Nenseth, Judith M. Müller, Sylvia Urban, Dominica Willmann, Kerstin Petroll, Nadia Messaddeq, Laura Arrigoni, Thomas Manke, Jan-Wilhelm Kornfeld, Jens C. Brüning, Vyacheslav Zagoriy, Michael Meret, Jörn Dengjel, Toufike Kanouni, and Roland Schüle

Supplemental Informations

Lsd1 ablation triggers metabolic reprogramming of brown adipose tissue

Delphine Duteil, Milica Tosic, Franziska Lausecker, Hatice Z. Nenseth, Judith M. Müller, Sylvia Urban, Dominica Willmann, Kerstin Petroll, Nadia Messaddeq, Laura Arrigoni, Jan-Wilhelm Kornfeld, Jens C. Brüning, Vyacheslav Zagoriy, Michael Meret, Jörn Dengjel, Thomas Manke, and Roland Schüle

Supplemental Figures and Legends

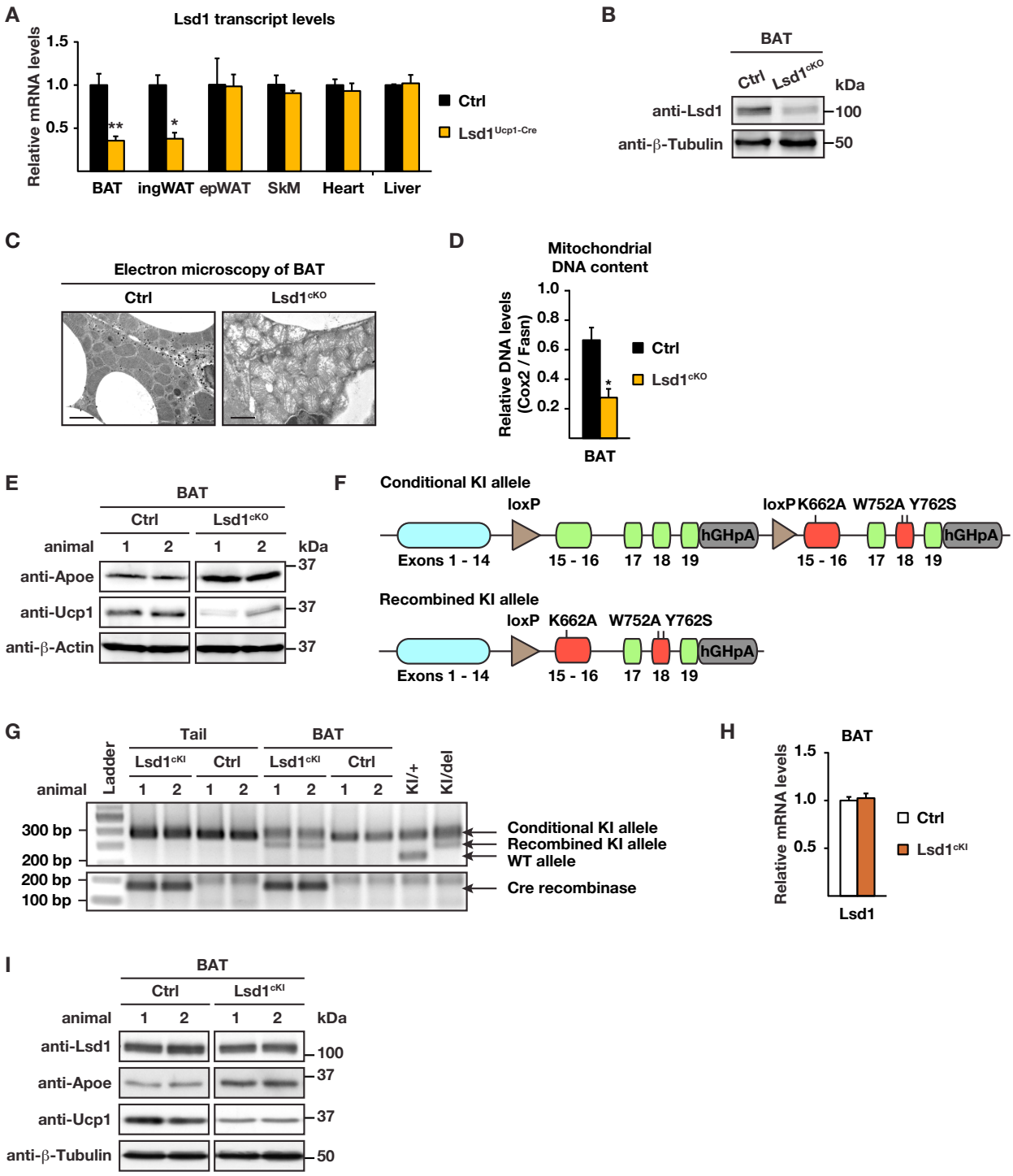

Figure S1 (related to Figure 1). Lsd1 represses the expression of WAT-selective genes in BAT.
(A) Relative Lsd1 mRNA levels in interscapular brown adipose tissue (BAT), inguinal white adipose tissue (ingWAT), epididymal white adipose tissue (epWAT), skeletal muscle (SkM), heart, and liver of control (Ctrl) and Lsd1^{cKO} mice (mean + SEM, *p<0.05, **p<0.01, Ctrl n = 9, Lsd1^{cKO} n = 7).
(B) Western blot analysis of Lsd1 in BAT of Ctrl and Lsd1^{cKO} mice. β-Tubulin was used as a loading control.
(C) Ultrastructure analysis of representative BAT sections of Ctrl and Lsd1^{cKO} mice. Scale bar: 2 µm.
(D) Ratio of mitochondria to nuclear DNA content assessed by quantitative PCR of the mitochondria-encoded Cox2 and the nuclear-encoded Fasn gene in BAT of Ctrl and Lsd1^{cKO} mice (mean + SEM, *p<0.05, n = 5).
(E) Western blot analysis of Apoe and Ucp1 in BAT of Ctrl and Lsd1^{cKO} mice. β-Actin was used as a loading control.
(F) Scheme depicting the *Lsd1* knock-in (KI) allele.
(G) Genotyping of mouse tail and BAT biopsies of Ctrl and Lsd1^{cKO} mice for the presence of Lsd1 conditional or recombined KI alleles (upper panel), or Ucp1-Cre recombinase (lower panel) by semi-quantitative PCR.
(H) Relative Lsd1 mRNA levels in BAT of Ctrl and Lsd1^{cKI} mice (mean + SEM, Ctrl n = 7, Lsd1^{cKI} n = 6).
(I) Western blot analysis of Lsd1, Apoe, and Ucp1 in BAT of Ctrl and Lsd1^{cKI} mice. β-Tubulin was used as a loading control.

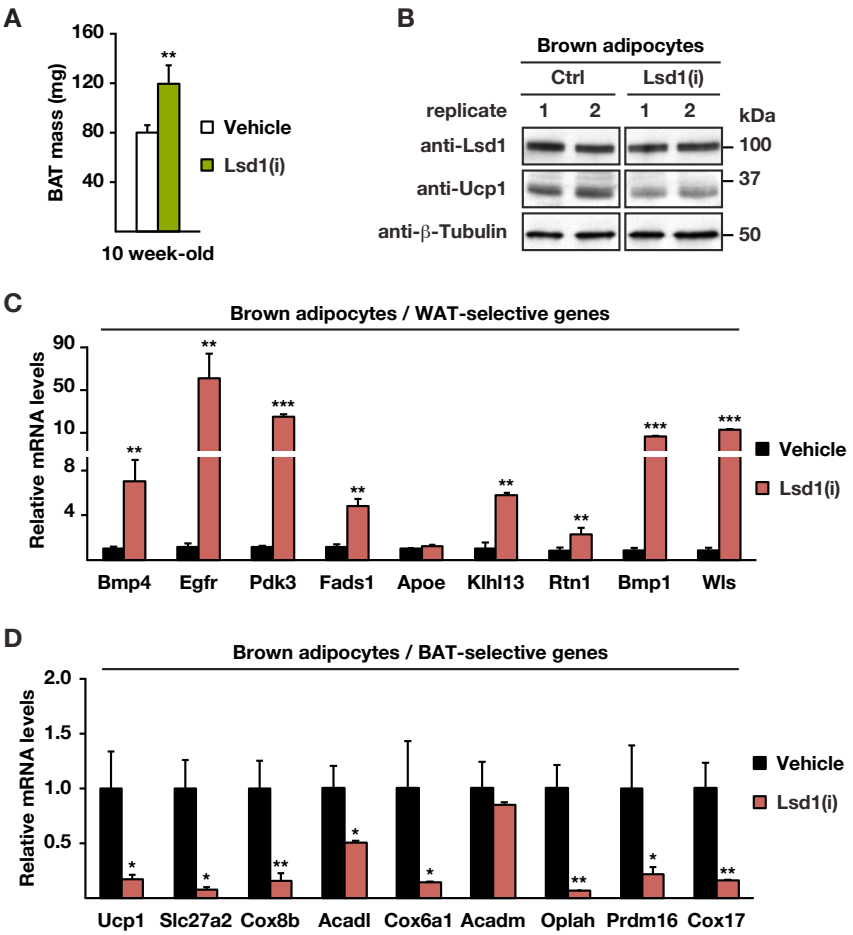

Figure S2 (related to Figure 2). The demethylase activity of Lsd1 is required to maintain BAT properties.
(A) Mass of BAT of 10 week-old mice treated with vehicle or Lsd1-specific inhibitor [Lsd1(i)] (mean + SEM, **p<0.01, vehicle n = 6, Lsd1(i) n = 7).
(B) Western blot analysis of Lsd1 and Ucp1 in brown adipocytes treated with vehicle or Lsd1(i). β-Tubulin was used as a loading control.
(C-D) Relative mRNA levels of (C) WAT- and (D) BAT-selective genes in brown adipocytes treated with vehicle or Lsd1(i) (mean + SEM, *p<0.05, **p<0.01, ***p<0.001, n = 6).

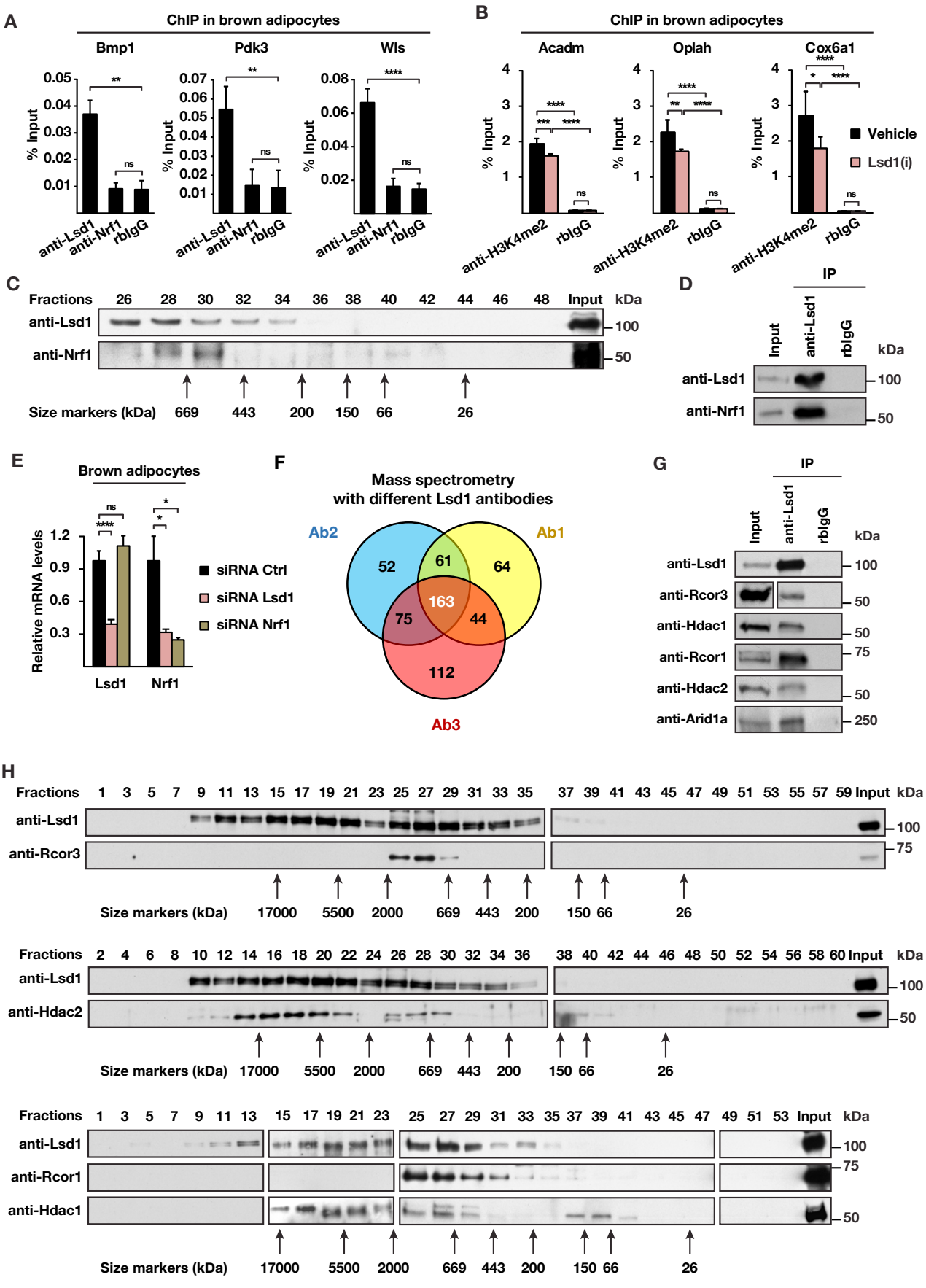
A
ChIP in brown adipocytes
Bmp1
Pdk3
Wls
% Input
anti-Lsd1
anti-Nrf1
rbIgG
B
ChIP in brown adipocytes
Acadm
Oplah
Cox6a1
anti-H3K4me2
rbIgG
Vehicle
Lsd1(i)
C
Fractions
Input
kDa
anti-Lsd1
anti-Nrf1
Size markers (kDa)
669
443
200
150
66
26
D
IP
Input
anti-Lsd1
rbIgG
E
Brown adipocytes
Relative mRNA levels
siRNA Ctrl
siRNA Lsd1
siRNA Nrf1
Lsd1
Nrf1
F
Mass spectrometry
with different Lsd1 antibodies
Ab1
Ab2
Ab3
52
61
64
163
75
44
112
G
anti-Rcor3
anti-Hdac1
anti-Rcor1
anti-Hdac2
anti-Arid1a
H
anti-Hdac1
17000
5500
2000

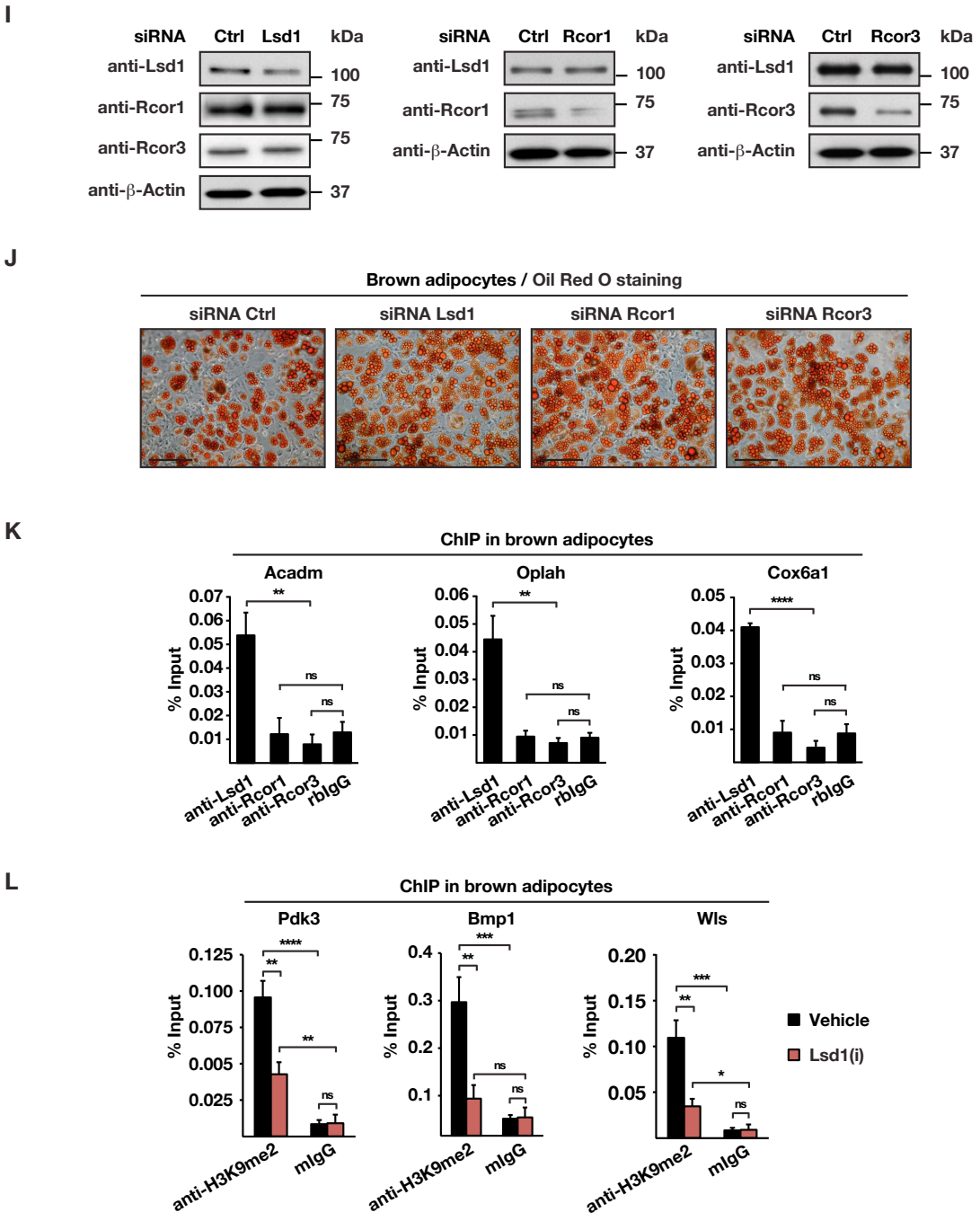

Figure S3 (related to Figure 3). Lsd1 regulates the brown fat program through a dual mechanism

(A) ChIP analysis to detect promoter occupancy performed with anti-Lsd1 and anti-Nrf1 antibodies or rabbit IgG (rbIgG) in brown adipocytes for indicated genes. The precipitated chromatin was quantified by qPCR analysis with primers flanking Lsd1-binding sites in the indicated genes (mean + SEM, n = 3).

(B) ChIP analysis to detect promoter occupancy performed with anti-H3K4me2 antibody or rbIgG in brown adipocytes treated with Lsd1(i) or vehicle. The precipitated chromatin was quantified by qPCR analysis with primers flanking Lsd1-binding sites in the indicated genes (mean + SEM, n = 3).

(C) Western blot analysis of individual fractions of brown adipocyte nuclear extracts obtained after gel filtration. Membranes were decorated with Lsd1 or Nrf1 antibody.

(D) Immunoprecipitation of Nrf1 with Lsd1 antibody from BAT nuclear extracts. Membranes were decorated with Lsd1 or Nrf1 antibody. Rabbit IgG (rbIgG) served as a control.

(E) Relative mRNA levels of Lsd1 and Nrf1 in brown adipocytes transfected with siRNA Ctrl, siRNA Lsd1, or siRNA Nrf1 (mean + SEM, n = 3). In agreement with previous data (Duteil et al., 2014), knock-down of Lsd1 results in reduced mRNA levels of Nrf1.

(F) Venn diagram depicting the overlap between Lsd1 interacting proteins identified by immunoprecipitation using three different Lsd1 antibodies followed by mass spectrometry. Ab1 and Ab2 correspond to 2 homemade anti-Lsd1 antibodies (see Experimental procedures for details) and Ab3 corresponds to the L-4481 (Sigma) anti-Lsd1 antibody.

(G) Immunoprecipitation of components of the CoREST complex with Lsd1 antibody from BAT nuclear extracts. Membranes were decorated with the indicated antibodies. Rabbit IgG (rbIgG) served used as a control.
(H) Western blot analysis of individual fractions of brown adipocyte nuclear extracts obtained after gel filtration. Membranes were decorated with the indicated antibodies.
(I) Western blot analysis of Lsd1, Rcor1, and Rcor3 in brown adipocytes transfected with siRNA Ctrl, siRNA Lsd1, siRNA Rcor1, or siRNA Rcor3. β-Tubulin was used as a loading control.
(J) Oil red O staining of brown adipocytes transfected with siRNA Ctrl, siRNA Lsd1, siRNA Rcor1, or siRNA Rcor3. Scale bar: 50 μm.
(K-L) ChIP analysis to detect promoter occupancy performed with (K) anti-Lsd1, anti-Rcor1, and anti-Rcor3 antibody or rbIgG, and (L) anti-H3K9me2 antibody or mIgG in brown adipocytes treated with Lsd1(i) or vehicle. The precipitated chromatin was quantified by qPCR analysis with primers flanking Lsd1-binding sites in the indicated genes (mean + SEM, n = 3).
(A), (E), (K): one-way ANOVA; (B), (L): two-way ANOVA; *p<0.05, **p<0.01, ***p<0.001, ****p<0.0001.

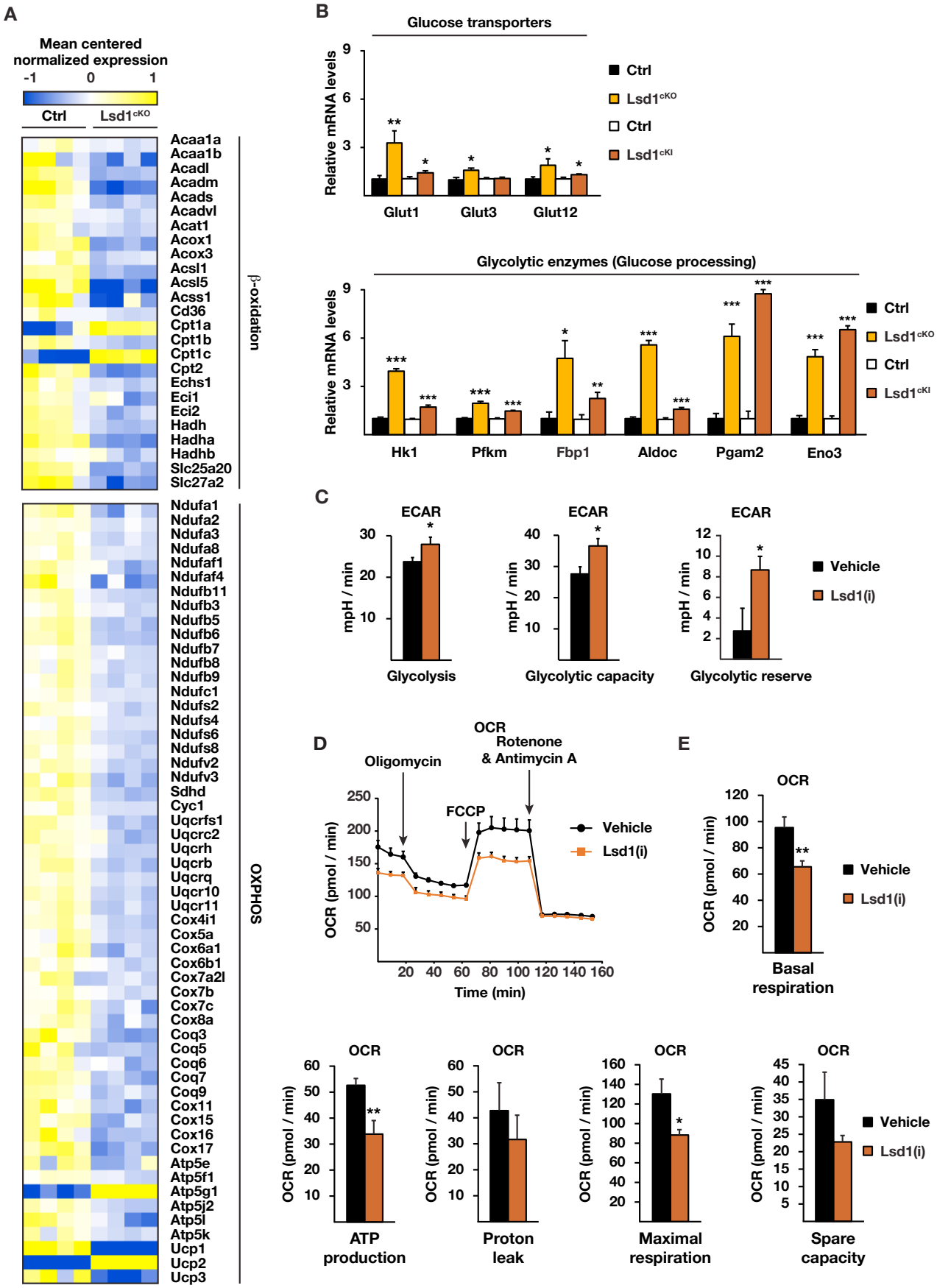
A
Mean centered normalized expression
-1
0
1
Ctrl
Lsd1cKO
Acaa1a
Acaa1b
Acadl
Acadm
Acads
Acadvl
Acat1
Acox1
Acox3
Acsl1
Acsl5
Acss1
Cd36
Cpt1a
Cpt1b
Cpt1c
Cpt2
Echs1
Eci1
Eci2
Hadh
Hadha
Hadhb
Slc25a20
Slc27a2
β-oxidation
Ndufa1
Ndufa2
Ndufa3
Ndufa8
Ndufaf1
Ndufaf4
Ndufb11
Ndufb3
Ndufb5
Ndufb6
Ndufb7
Ndufb8
Ndufb9
Ndufc1
Ndufs2
Ndufs4
Ndufs6
Ndufs8
Ndufv2
Ndufv3
Sdhd
Cyc1
Uqcrfs1
Uqcrc2
Uqcrh
Uqcrb
Uqcrq
Uqcr10
Uqcr11
Cox4i1
Cox5a
Cox6a1
Cox6b1
Cox7a2l
Cox7b
Cox7c
Cox8a
Coq3
Coq5
Coq6
Coq7
Coq9
Cox11
Cox15
Cox16
Cox17
Atp5e
Atp5f1
Atp5g1
Atp5j2
Atp5l
Atp5k
Ucp1
Ucp2
Ucp3
OXPHOS
B
Glucose transporters
Relative mRNA levels
Ctrl
Lsd1cKO
Ctrl
Lsd1cKI
Glut1
Glut3
Glut12
Glycolytic enzymes (Glucose processing)
Hk1
Pfkm
Fbp1
Aldoc
Pgam2
Eno3
C
ECAR
mpH / min
Glycolysis
Glycolytic capacity
Glycolytic reserve
Vehicle
Lsd1(i)
D
OCR
Oligomycin
Rotenone & Antimycin A
FCCP
OCR (pmol / min)
Time (min)
E
Basal respiration
ATP production
Proton leak
Maximal respiration
Spare capacity

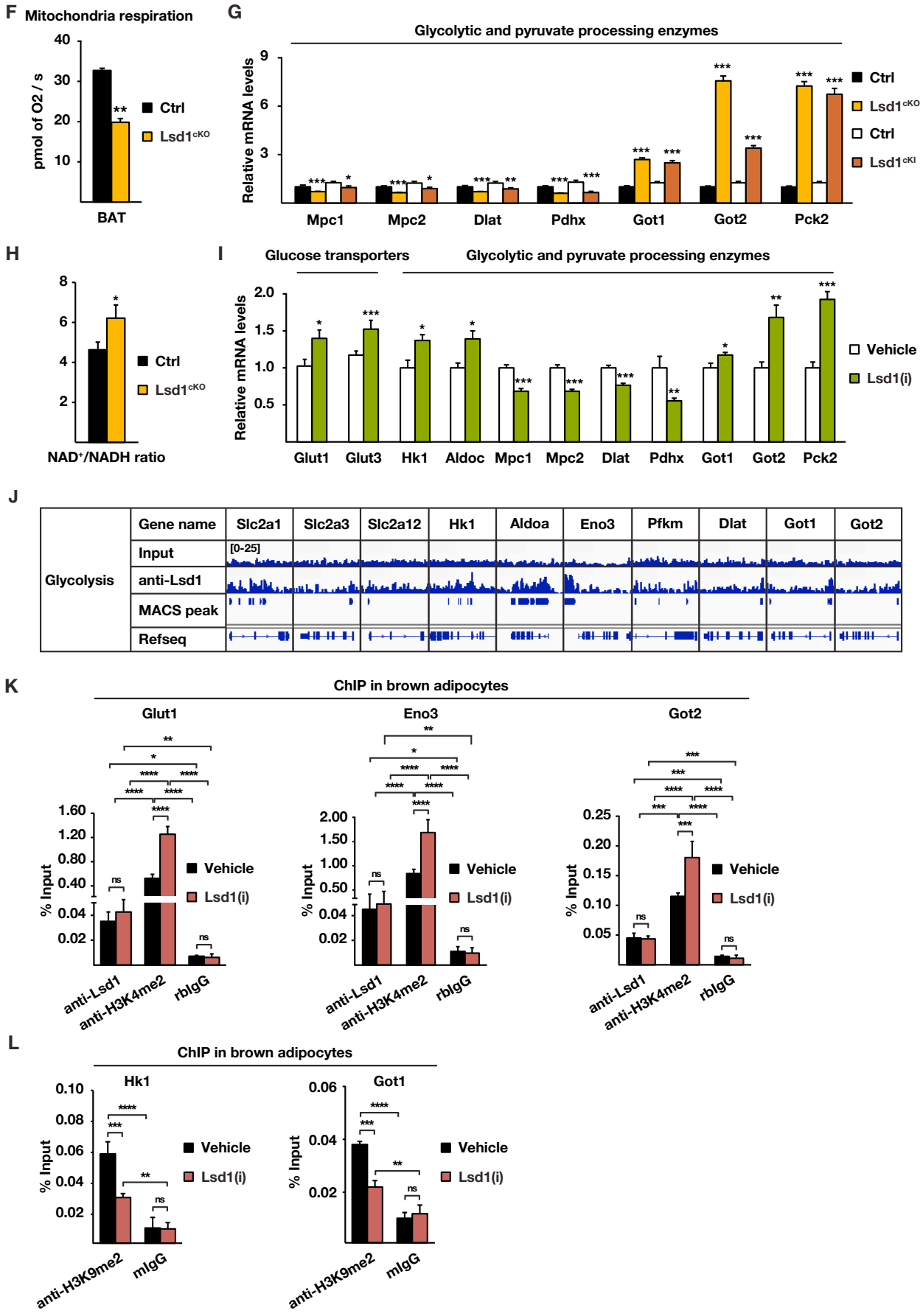

Figure S4 (related to Figure 4). Lsd1 represses glycolysis in BAT.
(A) Heatmaps depicting mRNA levels of genes involved in β-oxidation and oxidative phosphorylation (OXPHOS) in BAT of 10 week-old control (Ctrl) and Lsd1^{cKO} mice.

(B) Relative mRNA levels of genes encoding glucose transporters and glycolytic enzymes in BAT of Ctrl, Lsd1^{cKO}, and Lsd1^{cKI} mice [mean + SEM, *p<0.05, **p<0.01, ***p<0.001, Ctrl (black bars) n = 9, Lsd1^{cKO} (orange bars) n = 7, Ctrl (white bars) n = 7, and Lsd1^{cKI} (red bars) n = 6].
(C) Glycolysis, maximal glycolytic capacity and glycolytic reserve deduced from extracellular acidification rate (ECAR) (mean + SEM, *p<0.05, n = 6).
(D-E) Oxygen consumption rate (OCR) of vehicle- or Lsd1(i) treated brown adipocytes determined by the Seahorse Extracellular Flux Analyzer (mean + SEM, *p<0.05, n = 9).
(F) Mitochondrial respiration of BAT extracts from Ctrl and Lsd1^{cKO} mice assessed with a high-resolution respiratory Oxygraph-2K system (mean + SEM, **p<0.01, n = 5).
(G) Relative mRNA levels of genes encoding glycolytic and pyruvate processing enzymes in BAT of Ctrl, Lsd1^{cKO}, and Lsd1^{cKI} mice [mean + SEM, *p<0.05, **p<0.01, ***p<0.001, Ctrl (black bars) n = 9, Lsd1^{cKO} (orange bars) n = 7, Ctrl (white bars) n = 7, and Lsd1^{cKI} (red bars) n = 6].
(H) Determination of the NAD^+/NADH ratio in BAT of Ctrl and Lsd1^{cKO} mice at 10 weeks of age (mean + SEM, **p<0.01, ***p<0.001, n = 6).
(I) Relative mRNA levels of selected genes encoding glucose transporters, glycolytic, and pyruvate processing enzymes in BAT of mice treated with vehicle or Lsd1(i) [mean + SEM, *p<0.05, **p<0.01, ***p<0.001, Vehicle n = 6, Lsd1(i) n = 7].
(J) Localization of Lsd1 at the promoter of representative genes encoding glucose transporters, glycolytic and pyruvate processing enzymes in brown adipocytes.
(K-L) ChIP analysis to detect promoter occupancy performed with (K) anti-Lsd1 and anti-H3K4me2 antibody, or rbIgG or (L) anti-H3K9me2 antibody, or mIgG in brown adipocytes treated with vehicle or Lsd1(i). The precipitated chromatin was quantified by qPCR analysis with primers flanking Lsd1-binding sites in the indicated genes (mean + SEM, two-way ANOVA, ns: p>0.05, *p<0.05, **p<0.01, ***p<0.001, ****p<0.0001, n = 3).

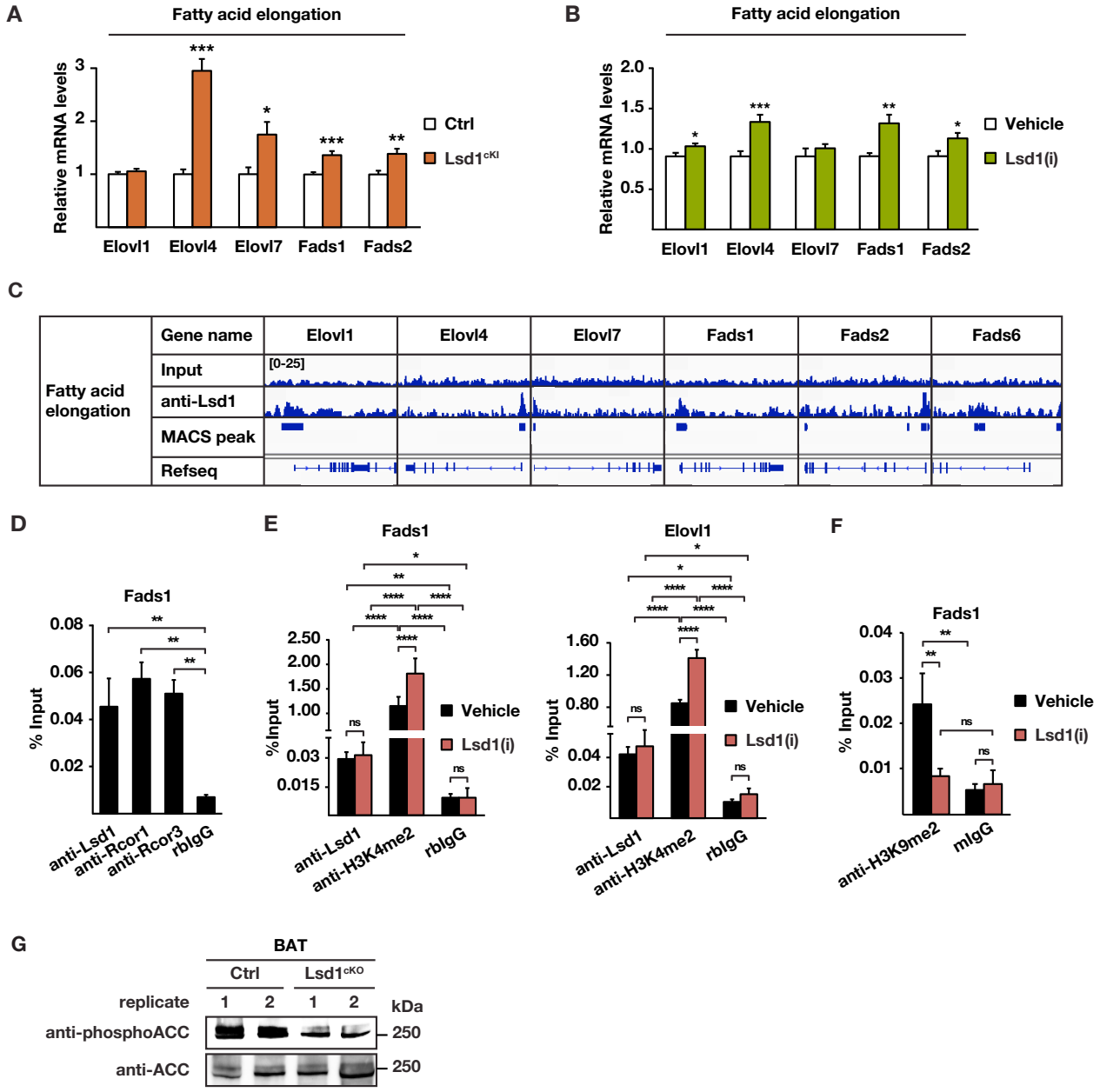

Figure S5 (related to Figure 5). Lsd1 limits fat accumulation in BAT.
(A-B) Relative mRNA levels of indicated enzymes involved in fatty acid elongation in BAT of (A) Ctrl and Lsd1^{cKI} mice and (B) mice treated with vehicle or Lsd1(i) [(A-B) mean + SEM, *p<0.05, **p<0.01, ***p<0.001; (A) Ctrl n = 7, Lsd1^{cKI} n = 6; (B) Vehicle n = 6, Lsd1(i) n = 7].
(C) Localization of Lsd1 at the promoter of representative genes encoding enzymes involved in fatty acid elongation in brown adipocytes.
(D-F) ChIP analysis to detect promoter occupancy performed with with (D) anti-Lsd1, anti-Rcor1, and anti-Rcor3 antibody or rbIgG in brown adipocytes, (E) anti-Lsd1 and anti-H3K4me2 antibody, or rbIgG, or (F) anti-H3K9me2 antibody, or mIgG in brown adipocytes treated with vehicle or Lsd1(i). The precipitated chromatin was quantified by qPCR analysis with primers flanking Lsd1-binding sites in the indicated genes (mean + SEM, (D) one-way ANOVA, (E-F) two-way ANOVA, ns: p>0.05, *p<0.05, **p<0.01, ***p<0.001, ****p<0.0001, n = 3).
(G) Western blot analysis of phosphor-ACC and total ACC in BAT of Ctrl and Lsd1^{cKO} mice.

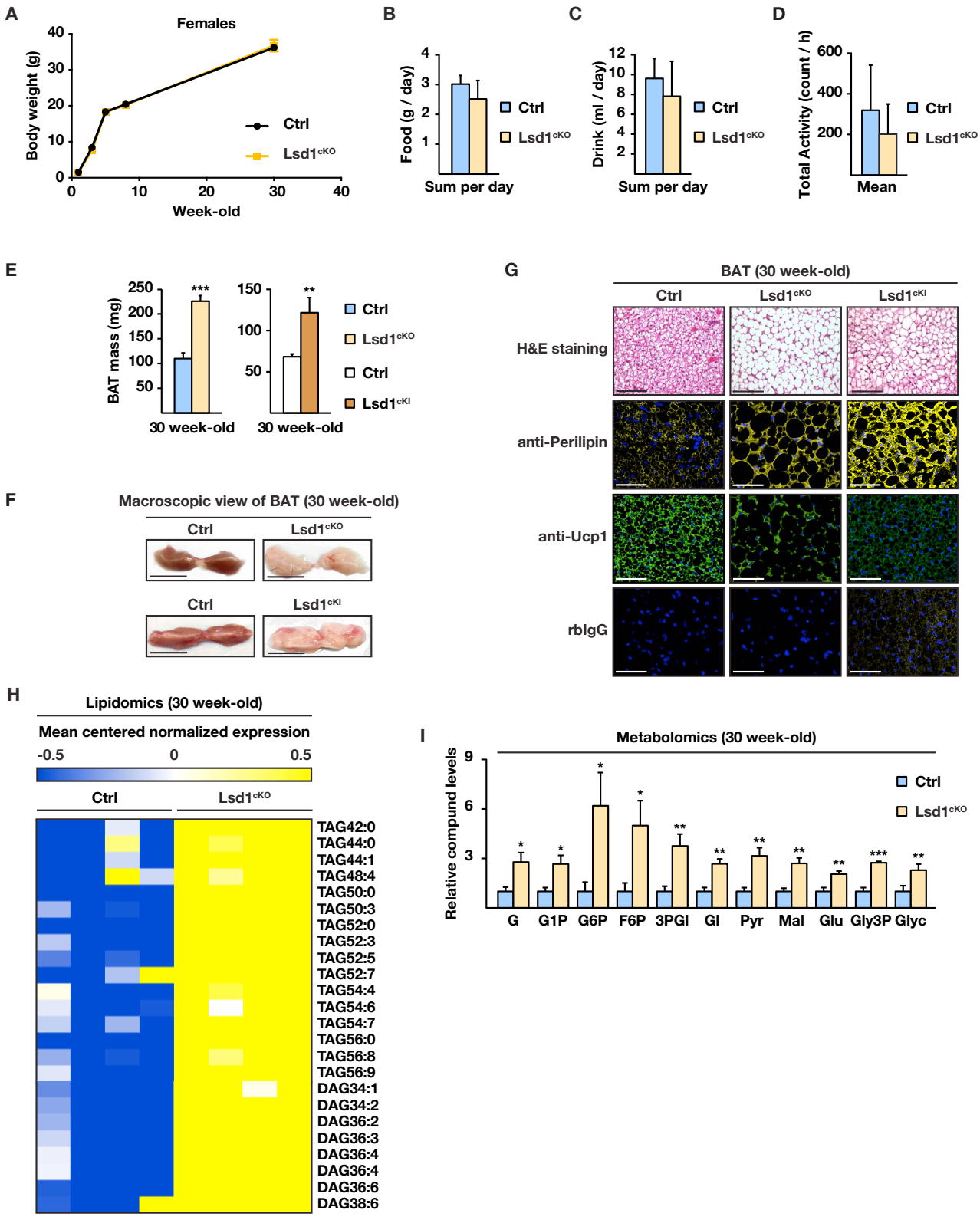
A
Females
Body weight (g)
Week-old
Ctrl
Lsd1cKO
B
Food (g / day)
Sum per day
C
Drink (ml / day)
Sum per day
D
Total Activity (count / h)
Mean
E
BAT mass (mg)
30 week-old
30 week-old
F
Macroscopic view of BAT (30 week-old)
G
BAT (30 week-old)
Lsd1cKI
H&E staining
anti-Perilipin
anti-Ucp1
rbIgG
H
Lipidomics (30 week-old)
Mean centered normalized expression
TAG42:0
TAG44:0
TAG44:1
TAG48:4
TAG50:0
TAG50:3
TAG52:0
TAG52:3
TAG52:5
TAG52:7
TAG54:4
TAG54:6
TAG54:7
TAG56:0
TAG56:8
TAG56:9
DAG34:1
DAG34:2
DAG36:2
DAG36:3
DAG36:4
DAG36:4
DAG36:6
DAG38:6
I
Metabolomics (30 week-old)
Relative compund levels
G
G1P
G6P
F6P
3PGl
Gl
Pyr
Mal
Glu
Gly3P
Glyc

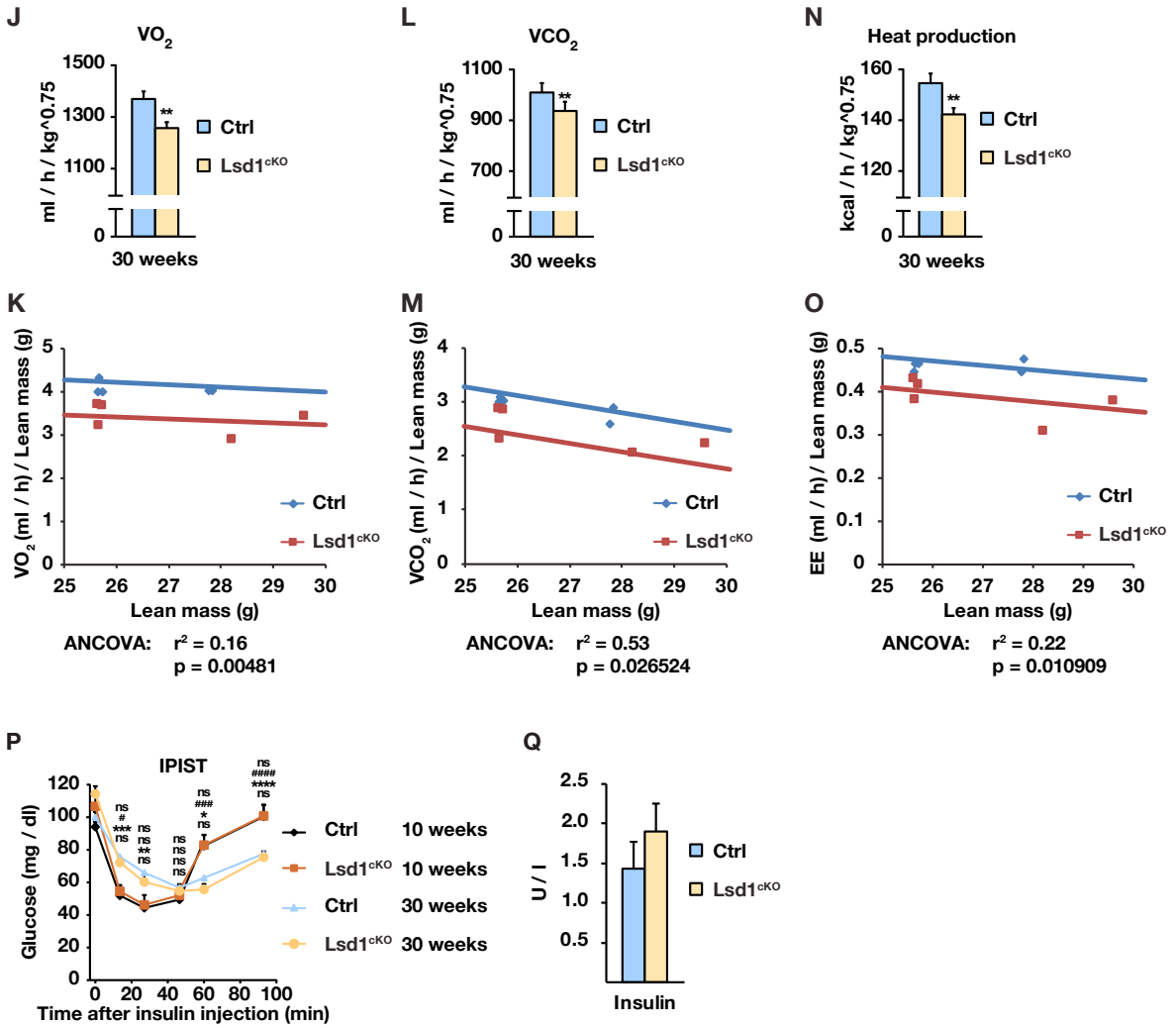

Figure S6 (related to Figure 6). Lsd1^{cKO} mice have a higher glucose uptake despite an increased body weight.
(A) Body weight of control and Lsd1^{cKO} female mice at indicated age (mean + SEM; two-way ANOVA with repeated measures; factor interaction: $p_{genotype/time}$: ns; Ctrl n = 6, Lsd1^{cKO} n = 6).
(B-D) (B) Food consumption, (C) drink consumption, and (D) total activity of 30 week-old control (Ctrl) and Lsd1^{cKO} mice (mean + SEM, Ctrl n = 9, Lsd1^{cKO} n = 7).
(E-F) (E) Mass and (F) macroscopic view of BAT of 30 week-old Ctrl, Lsd1^{cKO}, and Lsd1^{cKI} mice [(D) mean + SEM, **p<0.01, ***p<0.001, Ctrl n = 9, Lsd1^{cKO} n = 7, and Ctrl n = 7, Lsd1^{cKI} n = 6].
(G) H&E staining and perilipin or Ucp1 immunofluorescence of representative sections of BAT of 30 week-old Ctrl, Lsd1^{cKO}, and Lsd1^{cKI} mice. Nuclei were counterstained with DAPI. Rabbit IgG (rbIgG) was used as negative control.
(H) Lipidomic analysis of BAT from 30 week-old Ctrl and Lsd1^{cKO} mice (mean + SEM, n = 5).
(I) Relative abundance of indicated metabolites in BAT of Ctrl and Lsd1^{cKO} mice. G: glucose, G1P: glucose-1-phosphate, G6P: glucose-6-phosphate, F6P: fructose-6-phosphate, 3PGl: 3-phosphoglycerate, Gl: glycerate, Pyr: pyruvate, Mal: malate, Glu: glutamate, Gly3P: glycerol-3-phosphate, Glyc: glycerol (mean + SEM, n = 5, *p<0.05, **p<0.01, ***p<0.001).
(J-O) (J-K) VO_2, (L-M) VCO_2, and (N-O) energy expenditure of 30 week-old control and Lsd1^{cKO} mice represented related to the metabolic body weight (J, L, and N) (mean + SEM, *p<0.05, **p<0.01, Ctrl n = 8, Lsd1^{cKO} n = 7) or as a linear regression (K, M, and O) for which an ANCOVA analysis was performed.
(P) Intraperitoneal insulin sensitive test (IPIST) for 10 week-old or 30 week-old control and Lsd1^{cKO} mice starved for 6 hours prior to analysis (mean + SEM, two-way ANOVA, Ctrl 10 week-old vs Lsd1^{cKO} 10 week-old: ns p>0.05; Ctrl 10 week-old vs Ctrl 30 week-old: **p<0.01, ***p<0.001, ****p<0.0001; Lsd1^{cKO} 10 week-old vs Lsd1^{cKO} 30 week-old: # p<0.05, ### p<0.001, #### p<0.0001; Ctrl 30 week-old vs Lsd1^{cKO} 30 week-old: ns p>0.05; Ctrl n = 8, Lsd1^{cKO} n = 7).
(Q) Serum insulin levels of 30 week-old control (Ctrl) and Lsd1^{cKO} mice (mean + SEM, Ctrl n = 9, Lsd1^{cKO} n = 7).
Scale bars: (F) 7 mm, (G) H&E staining 100 µm, immunofluorescence 20 µm.

Supplemental Tables

Table S1 (related to Figure 1). mRNA ratios [represented as log(fold change), logFC] for BAT- (yellow) and WAT-selective (bleu) genes in BAT and WAT of 10 week-old control mice (BAT / WAT) and in BAT of 10 week-old Lsd1^{cKO} and control mice (cKO / Ctrl).

Table S2 (related to Figure 3). List of the 163 Lsd1 interacting proteins identified by immunoprecipitation followed by mass-spectrometry. The calculation of log2-value is described in Materials and Methods.

Gene	Sense	Primer 5'-3'
***Lsd1* WT/L2**	fw	CCTCAGTAGGCCTGGTTTGT
***Lsd1* WT/L2**	rev	TTGGTTTTGGTTGACCCTTC
***Lsd1* L-**	fw	CCGTGGAAATTCGTGCACTC
***Lsd1* L-**	rev	GCAGGCGGTTTGAAATGTATTC
***Lsd1* WT/KI**	fw	CCAGCTGCTTGTTGGTGC
***Lsd1* WT/KI**	rev	TGGAGTGAAGTGGTTACCTGC
Ucp1-Cre	fw	CCTCTGCACTGGCACTACCT
Ucp1-Cre	rev	TCTTCTTCTTGGGCACCATC

Table S3 (related to Figure S1). Primers used for genotyping

Gene	Sense	Primer 5'-3'
Tbp	fw	GAAGCTGCGGTACAATTCCAG
Tbp	rev	CCCCTTGTACCCTTCACCAAT
36b4	fw	GCGTCCTGGCATTGTCTGT
36b4	rev	GCAAATGCAGATGGATCAGCC
Hprt	fw	AGGGCATATCCAACAACAAACTT
Hprt	rev	GTTAAGCAGTACAGCCCCAAA
Lsd1	fw	GTGTTCTGGGACCCAAGTGT
Lsd1	rev	TAATGCCAGCAGCTTCTCCT
Bmp4	fw	GCTGGAATGATTGGATTGTGG
Bmp4	rev	ATGGCATGGTTGGTTGAGTTG
Egfr	fw	ACACTGCTGGTGTTGCTGAC
Egfr	rev	CCCAAGGACCACTTCACAGT
Pdk3	fw	TTTGAGAGGCTGCCAGTTTT
Pdk3	rev	CGTCTCTGGTTGACTTGCAG
Fads1	fw	AAGGCCAACCACCTCTTCTT
Fads1	rev	ACTGACAGGTGCCCAAAGTC
Apoe	fw	GGTTCGAGCCAATAGTGGAA
Apoe	rev	TATTAAGCAAGGGCCACCAG
Klhl13	fw	AGAATTGGTTGCTGCAATACTCC
Klhl13	rev	AAGGCACAGTTTCAAGTGCTG
Rtn1	fw	TCCGCATCTACAAGTCCGTT
Rtn1	rev	AAAAGCCTCCGTAGCTCCTT
Bmp1	fw	CAAGGCCCACTTCTTCTCAG
Bmp1	rev	TTGTGTTCACAGCCAGCTTC
Wls	fw	ATTTGACTGGACCTGGATGC
Wls	rev	TTCCAGTACCCTGCAATGTG
Ucp1	fw	TGGCAAAAACAGAAGGATT
Ucp1	rev	CGAGTCGCAGAAAAGAAGC
Slc27a2	fw	ATGCCGTGTCCGTCTTTTAC
Slc27a2	rev	CGATGATGATTGATGGTTGC
Acadm	fw	GGATGACGGAGCAGCCAATG
Acadm	rev	ATACTCGTCACCCTTCTTCT
Oplah	fw	CTTCACGCACGTCTCCTTGT
Oplah	rev	GCATCTGCACAGGCCGTAT
Acadl	fw	TTGGTGGGGACTTGCTCTCA
Acadl	rev	CTGTTCTTTTGTGCCGTAAT
Cox6a1	fw	TGCTCAACGTGTTCCTCAAG
Cox6a1	rev	TAAGGGTCCAAAACCAGTGC
Prdm16	fw	CCCCCAACGCTCTCGGATCC
Prdm16	rev	CCGAAGCAGCGGTTGCACAG
Cox17	fw	ATAGTTGCTTTCGCCTGGAA
Cox17	rev	ACAAAGTAGGCCACCACGTC
Elovl1	fw	TTCCAACTTCGAGGCTTCAT
Elovl1	rev	GCTCAATGACCTTGGAAAGC
Elovl4	fw	ACTATGGGCTGACTGCGTTC
Elovl4	rev	TTCCGGTTTTTGACTGCTTC
Elovl7	fw	TCATCCTGGGCCTCTATGTC
Elovl7	rev	ACCATCCTCATTGCTCTTGG
Fads2	fw	GCTCTCAGATCACCGAGGAC
Fads2	rev	AGTGCCGAAGTACGAGAGGA

Gene	Sense	Primer 5'-3'
Hk1	fw	TGGACAAAGGGATTCAAAGC
Hk1	rev	CTCCACCATCTCCACGTTTT
Pfkm	fw	GCTGTGGTCCGAGTTGGTAT
Pfkm	rev	CTCTCGGAAGTCCTTGCATC
Fbp1	fw	CCATCATAATCGAACCTGAG
Fbp1	rev	CTTCTCAGAAGGCTCATCAG
Aldoc	fw	CTGCTCAAGCCCAATATGGT
Aldoc	rev	CTTCACTCTGACCCCCAGAC
Pgam2	fw	ACACCTCCATCAGCAAGGAC
Pgam2	rev	GGGCTGCAATAAGCACTCTC
Eno3	fw	CTCCGAGATGGAGACAAAGC
Eno3	rev	CGTCCAGCTCAATCATGAAC
Ldha	fw	AGACAAACTCAAGGGCGAGA
Ldha	rev	CAGCTTGCAGTGTGGACTGT
Mpc1	fw	ACTTTCGCCCTCTGTTGCTA
Mpc1	rev	AAGTCGTCCTCCCTGAATGA
Mpc2	fw	TGTTGCTGCCAAAGAAATTG
Mpc2	rev	GCTAGTCCAGCACACACCAA
Dlat	fw	TCCAAAGCGAGAGAGGGTAA
Dlat	rev	AGCACCGATTGCCAGAATAC
Pdhx	fw	ATTCCCAAGGATGTCAGTGC
Pdhx	rev	CAGCTGGACTTAAGCGGAAC
Got1	fw	GCTGACTTCTTAGGGCGATG
Got1	rev	TAGCAATAGGGCCGAATGTC
Got2	fw	TTGATCCGTCCCCTGTATTC
Got2	rev	TTAGGCCGGTGAAACAGAAC
Pck2	Fw	GGGGTACCACTGGTGTACGA
Pck2	rev	TCTCTCCGGAACCAATTGAC
Glut1	fw	TCAACACGGCCTTCACTG
Glut1	rev	CACGATGCTCAGATAGGACATC
Glut3	fw	TTCTGGTCGGAATGCTCTTC
Glut3	rev	AATGTCCTCGAAAGTCCTGC
Glut12	fw	ACTATCCCAGCAACCCTCCT
Glut12	rev	AAACTCCTCCAGGGACTGGT
Ndufa6	fw	GTCACAGACCCCAGAGTGGT
Ndufa6	rev	TAACATGCACCTTCCCATCA
Sdha	fw	ACACAGACCTGGTGGAGACC
Sdha	rev	GGATGGGCTTGGAGTAATCA
Uqcrc1	fw	GACAACGTGACCCTCCAAGT
Uqcrc1	rev	ACTGGTACATAGGCGCATCC
Cox8b	fw	GAACCATGAAGCCAACGACT
Cox8b	rev	GCGAAGTTCACAGTGGTTCC
Atp5b	fw	GAGGGATTACCACCCATCCT
Atp5b	rev	CATGATTCTGCCCAAGGTCT
Cpt1b	fw	CAGCTGGCTGGTTGTTGTCA
Cpt1b	rev	TTGTCGGAAGAAGAAAATGC
Pgc1a	fw	AAGTGTGGAACTCTCTGGAACTG
Pgc1a	rev	GGGTTATCTTGGTTGGCTTTATG
Cox2	fw	CAGTCCCCTCCCTAGGACTT
Cox2	rev	TTTCAGAGCATTGGCCATAGAA
Fasn	fw	AGGATATGGAGAGGGCTGGT
Fasn	rev	ACCCAAGCATCATTTTCGTC

Table S4. Primers used for qPCR analysis

Gene	Sense	Primer 5'-3'
Acadm	fw	CTTCGTGTTGTGCCTGTGTT
Acadm	rev	GCCACTTCTCTCCAGTCACC
Oplah	fw	CAGGGGGAAAGTAGGAAAGG
Oplah	rev	CCAGGCTTGTGTGTCTGTGT
Cox6a1	fw	TTGCGAGCTTTTCTGGTTTT
Cox6a1	rev	GGGCACAACGGAAGAGAATA
Unrelated1	fw	AATGCCTCTCACGCTCAACT
Unrelated1	rev	AAGTGTGTGCCATCCTTTCC
Pdk3	fw	TTCCTTAAAGCCCCGGTAAC
Pdk3	rev	GGGAGGTCTAGAGCCCCTAA
Fads1	fw	ACGGTGAGAGCGGACAATAG
Fads1	rev	ATCCAACCCATGCTTGAGAC
Bmp1	fw	GTCTCTGTCGCTGTCCTTCC
Bmp1	rev	TTCTCAGCTCGGCTTCTAGC
Wls	fw	CTGGCTGTGGCTTGTGTAAA
Wls	rev	GGACAAGAGGCAAAAGCAAC
Unrelated2	fw	AGCCAGGGCTACACAGAGAA
Unrelated2	rev	AGATTCCTGCACCAAAGTGG
Slc2a1	fw	ATCAGAAAGGGACACGGATG
Slc2a1	rev	AAATCCTCCCGAGGAAAGAA
Slc2a12	fw	CTAGACCCAAATCCCGTTGA
Slc2a12	rev	CGCCGAAGAGGAACATTTTA
Hk1	fw	AAACTAGGCGGCTTCACAGA
Hk1	rev	GGGGACCATGAGCTCTTACA
Eno3	fw	GCGGAGAGAGTTACCGAGTG
Eno3	rev	TTCCTGCGTGAAGCCTAAGT
Got1	fw	CCGCAGTGAGCTTAAAGACC
Got1	rev	AGTCGGAAGGTTGTGATTGG
Got2	fw	GTAAGACGGCAGTGGATGGT
Got2	rev	CTTGCGAGTTTCCATGACCT
Elovl1	fw	CAGCCCTTAGTAGGCACAGC
Elovl1	rev	CACCCAGCTTCTTCTTGAGG

Table S5. Primers used for ChIP-qPCR analysis

Supplemental Experimental Procedures

Generation of conditional *Lsd1* knock-out and knock-in mice

All experiments were performed in C57/Bl6N background. The targeting strategy for the conditional deletion of the first exon of *Lsd1* (*Lsd1*^{tm1Schüle}) is available upon request (Zhu et al., 2014). Briefly, conditional *Lsd1* mice were mated with *Ucp1-Cre* mice to selectively ablate *Lsd1* in brown adipose tissue (Figures S1A and S1B). Homozygous conditional mice were used as controls. Mice were genotyped with primers for detection of conditional *Lsd1* alleles and *Cre* recombinase (Table S3).

Lsd1 knock-in (KI) mice were generated by Taconic [C57BL/6-Kdm1a$^{tm2931(K662A,\ W752A,\ Y762S)Arte}$]. The targeting vector has been engineered as follows (Figure S1F). Wild-type *Lsd1* exons 15 to 19, including the complete 3' untranslated region (UTR), were flanked by *loxP* sites. An additional polyadenylation signal (hGHpA: human Growth Hormone polyadenylation signal) was inserted between the 3' UTR and the distal *loxP* site in order to prevent downstream transcription of the mutated *Lsd1* exons 15 to 19. The size of the *loxP*-flanked region is 5.1 kb. Exons 15 to 19, including the splice acceptor site of intron 14, were duplicated and inserted downstream of the distal *loxP* site. Intron 15 was removed from the wild-type and the duplicated region in order to create a fusion of exon 15/16. K662A mutation was introduced into the duplicated exon 15, W752A and Y762S mutations were introduced into the duplicated exon 18. A second hGHpA cassette was inserted downstream of the duplicated 3' UTR. Positive selection markers were flanked by *FRT* (Neomycin resistance) and *F3* (Puromycin resistance) sites, and inserted into intron 14 and downstream of the second hGHpA, respectively. The targeting vector has been generated using BAC clones from the C57BL/6J RPCIB-731 BAC library and transfected into the Taconic Artemis C57BL/6N Tac ES cell line. Homologous recombinant clones were isolated using double positive (NeoR and PuroR) selection (in order to increase the efficiency of co-integration of both *loxP* sites and the point mutations). The conditional KI allele was obtained after Flp-mediated deletion of the selection markers. This allele expresses wild-type Lsd1 protein. The presence of the first hGHpA cassette downstream of the wild-type exon 19 should prevent transcription of the mutated exons 15 to 19. Conditional *Lsd1*$^{KI/KI}$ mice were crossed to *Ucp1-Cre* mice to selectively express mutated Lsd1 in brown adipose tissue (Lsd1^{cKI} mice). Homozygous conditional *Lsd1*$^{KI/KI}$ mice were used as controls. Mice were genotyped with primers for detection of conditional KI alleles and *Cre recombinase* (Figure S1G and Table S3).

RNA preparation, qRT-PCR, and RNA sequencing (RNA-seq)

RNA was isolated with TRIzol Reagent (Invitrogen) and processed as described (Duteil et al., 2014). Data were analyzed using the standard curve method (Bookout et al., 2006). *36b4*, *Hprt*, or *β-actin* were used for normalization. Primer sequences are given in Table S4.

RNA samples were sequenced by the standard Illumina protocol to create raw sequence files (.fastq files). We annotated these reads to the mm10 build of the mouse genome using TopHat version 2. The aligned reads were counted with the homer software (analyze RNA) and DEGs were identified using EdgeR and DESeq version 1.8.3. Differentially regulated genes (reads > 50, $p < 0.01$) were further used for pathway analysis in WebGestalt (Heinz et al., 2010; Wang et al., 2013).

Protein analyses

Western blot analysis, co-immunoprecipitation assays, gel filtration, and mass spectrometry experiments were performed as described (Duteil et al., 2014; Metzger et al., 2016). For gel filtration, brown adipocytes were harvested and suspended in isolation buffer (10 mM HEPES-KOH, pH 7.9, 1.5 mM $MgCl_2$, 10 mM KCl, 0.5 mM DTT, and complete protease inhibitor cocktail, Roche), allowed to swell on ice for 10 min, and pelleted. Isolated nuclei were resuspended in 20 mM HEPES-KOH, pH 7.9, 25 % glycerol, 420 mM NaCl, 1.5 mM $MgCl_2$, 0.2 mM EDTA, 0.5 mM DTT, and complete protease inhibitor cocktail, incubated on ice for 20 min and centrifuged at 14,000 r.p.m. for 10 min. Nuclear complexes were separated by gel filtration on a Superose 6^{TM} 10/300 GL column (GE Healthcare) using the ÄKTA pure 25 system (GE Healthcare). The void volume was 7.2 mL. 60 fractions of 300 µL were collected from an elution volume of 4.8 mL. The gel filtration buffer was composed of 50 mM KCl, 50 mM $NaCH_3COOH$, pH 7.2 including protease inhibitors and phosphatase inhibitors (Roche Diagnostics). Column calibration was done using carbonic anhydrase (26 kDa), bovin serum albumin (66 kDa), alchol dehydrogenase (150 kDa), ☆-amylase (200 kDa), apoferritin (443 kDa), and thyroglobulin (669 kDa) as markers according to the method provided by the supplier. Western blot membranes were decorated using following antibodies: anti-Lsd1 [3544 , Schüle laboratory (Duteil et al., 2014), 1/1000], anti-Ucp1 (Abcam, ab10983, 1/1000), anti-Apoe (Santa Cruz, M-20, 1/200), anti-Nrf1 (Abcam, ab55744, 1/500), anti-Hdac1 (Abcam, ab7028-50, 1/1000), anti-Hdac2 (Santa Cruz, sc-7899, 1/2500), anti-Rcor1 (Abcam, ab32631, 1/400), anti-Rcor3 (Abcam, ab76921, 1/2000), anti-Arid1a (Santa Cruz, sc-373784, 1/200), anti-phosphoAcc (Cell signaling, 11818, 1/1000), anti-Acc (Cell signaling, 3676, 1/1000), anti-β-Tubulin (Sigma, T6074, 1/10000), and anti-β-Actin (Sigma, A1978, 1/10000). Secondary antibodies conjugated to horseradish peroxidase (GE Healthcare) were detected using an enhanced chemiluminescence detection system (GE Healthcare). For immunoprecipitation assay, 500 mg of

protein extracts were incubated with 5 µg of anti-Lsd1 (Sigma, L-4481) and processed as described (Metzger et al., 2010). Mass spectrometry experiments were performed as described (Metzger et al., 2016). Lsd1 antibodies used for immunoprecipitation were Sigma L-4481 (Ab3 in Figure S3F), and the two Lsd1 antibodies 20752 and 3544 (Ab1 and Ab2 in Figure S3F, respectively) that we previously characterized (Duteil et al., 2014). The number of peptides obtained for each protein after Lsd1 immunoprecipitation was subtracted from the number of peptides obtained with IgG. The resulting number was then normalized to the number of Lsd1 peptides on a log2 basis. The calculation of log2-value is presented in Table S2. GO cellular component analysis was performed using the Panther algorithm (Ashburner et al., 2000).

Primary cell isolation and cell culture

BAT was cut in small pieces and incubated with 2 mg/ml collagenase I (CLS-1, Worthington) for 45 min. The cell suspension was filtered through a 150 µm nylon mesh and the stromal-vascular fraction (SVF) was isolated by low-speed centrifugation. For FACS analysis, the erythrocyte-free SVF was incubated with a mix of antibodies against different surface markers as described previously (Duteil et al., 2014; Wu et al., 2012) and sorted using an Aria flow cytometer (BD Biosciences). Dead cells were removed using DAPI staining (1/10000). Primary adipocytes were cultured in DMEM High Glucose containing 20 % fetal calf serum (FCS) and 2 % of 1 M Hepes buffer in dishes coated with collagen. Alternatively, preiBA cells were cultured in DMEM containing sodium pyruvate and glutamine (GIBCO 11995-065) supplemented with 10 % FCS. Differentiation of primary adipocytes and preiBA cells was induced by treatment of confluent cells with an adipogenic mixture consisting of 850 nM insulin (Gibco), 1 µM dexamethasone (Calbiochem), 1 µM rosiglitazone (Cayman), 125 nM indomethacin (Sigma), 1 nM T3 (Sigma), and 500 µM isobutylmethylxanthine (Serva) in the presence of 10 % FCS. The differentiation medium was replaced 2 days later with medium supplemented with 10 % FCS, 850 nM insulin, and 1 nM T3 for 2 days. Subsequently, cells were cultured in the same medium for 4 more days and considered as differentiated. Differentiated cells were transfected with 1 mM siRNA against Lsd1, Nrf1, Rcor1, Rcor3, or unrelated control (Invitrogen) using Lipofectamine RNAimax (Invitrogen) according to the manufacturer's instructions. siRNA oligonucleotide sequences were as follows:
Lsd1 siRNA: 5'-CCCAAAGAUCCAGCUGACGUUUGAA-3';
Nrf1 siRNA: 5'-UAUGGUAGCCAUGUGUUCAGUUUGG-3';
Rcor1 siRNA: 5'-GCGCAGUCAAGAACGAGACAAUCUU-3';
Rcor3 siRNA: 5'-UCCCAGAUGCCAAAUUGGAUGAAUA-3';
unrelated control siRNA: 5'-UUCUUAGCAAGACUGGUCUCUAGGG-3'.
Lsd1 inhibitor QC6688 was applied to differentiated cells at 100 nM (in EtOH) for 3 days. EtOH was used as a vehicle. Brown adipocytes were either harvested and snap-frozen for RNA, protein, and chromatin immunoprecipitation experiments, fixed for 1 h with 4 % PFA and stained with Oil Red O, or fixed for 5 min with 1 % PFA for chromatin immunoprecipitation experiments (see bellow).

Chromatin immunoprecipitation (ChIP) and ChIP sequencing (ChIP-seq)

Chromatin immunoprecipitation experiments were performed using anti-Lsd1 (20752, Schüle laboratory), anti-Nrf1 (Abcam, ab55744), anti-Rcor1 (Abcam, ab32631), anti-Rcor3 (Abcam, ab76921), H3K9me2 (Diagenode, Mab-154-050), or H3K4me2 (Diagenode, CS-035-100) antibodies, or a rabbit IgG negative control on protein G-Sepharose 4B (GE Healthcare) essentially as described (Metzger et al., 2008). For ChIP experiments, ChIPed DNA was processed by qPCR analyses with the primers described in Table S5. For ChIP-seq analysis, libraries were prepared from Lsd1-immunoprecipitated DNA according to standard methods. ChIP-seq libraries were sequenced using a HiSeq 2000 (Illumina) and mapped to the mm10 reference genome using bowtie 2 (Langmead et al., 2009). Data were analyzed using the peak finding algorithm MACS 1.41 (Zhang et al., 2008) using input as control. All peaks with a FDR greater than 0.3 % were excluded from further analysis. The uniquely mapped reads were used to generate the genome-wide intensity profiles, which were visualized using the IGV genome browser (Thorvaldsdottir et al., 2012). HOMER (Heinz et al., 2010) was used to annotate peaks, to calculate overlaps between different peak files, and for motif searches. The genomic features (promoter, exon, intron, 3' UTR, and intergenic regions) were defined and calculated using Refseq and HOMER.

Histological and immunofluorescence analysis

Tissues were fixed in 10 % buffered formalin and embedded in paraffin. 5 µm paraffin sections were deparaffinised and rehydrated. Hematoxylin and eosin staining was performed as described (Duteil et al., 2014). For immunofluorescence analyses, rehydrated sections were boiled in antigen unmasking solution (Tris buffer pH 9) for 20 min, cooled to room temperature, washed 3 times with PBS, 0.1 % Triton-X100 for 5 min, blocked for 1 h in 5 % FBS (Gibco, 10270-106) in PBS, 0.1 % Triton-X100, and incubated overnight at 4°C with anti-Lsd1 (1/1000), anti-Ucp1 (Abcam, ab10983, 1/500), or anti-Perilipin (Abcam, ab3526, 1/400) antibodies. Slides were then incubated with secondary antibody conjugated to Alexa488 (Invitrogen, 1/400) and mounted in aqueous

medium (Fluoromount-G, SouthernBiotech, 0100-01) with DAPI (Sigma, D-9542, 1/1000). Ultrastructural analyses were performed as described (Duteil et al., 2014).

Measuring activities of metabolic enzymes

Glucose uptake, hexokinase, phosphofructokinase, enolase, lactate dehydrogenase, glutamate oxaloacetic transaminase, NAD^+/NADH ratio, hormone-sensitive lipase, LPL, and fatty acid synthase activities were assessed by the Glucose Uptake Assay Kit (ab136955, abcam), Hexokinase Colorimetric Assay Kit (MAK091, Sigma), the Phosphofructokinase Colorimetric Assay Kit (MAK093, Sigma), the Enolase Activity Colorimetric/Fluorometric Assay Kit (K691-100, Bio Vision), the Lactate Dehydrogenase Activity Assay Kit (Sigma, MAK066), the Glutamate-oxaloacetate transaminase kit (K753-100, Bio Vision), the NAD/NADH Assay Kit (ab65348, abcam), the Lipase Activity Assay Kit (MAK046, Sigma), the LPL Activity Assay kit (MAK109, Sigma), and Fatty Acid Synthase ELISA kit (ABIN425666, antibodies-online), respectively. All activities were measured using 20-50 mg of BAT according to the manufacturer recommendations.

Metabolomic and lipidomic analyses

Tissue samples were grinded with a Retsch MM440 instrument and further extracted as described in (Giavalisco et al., 2009). LC-MS measurements were performed using a Waters ACQUITY UPLC system coupled to a Thermo-Fisher QExactive mass spectrometer. Lipophilic compounds were separated using a C8 and hydrophilic compounds using a C18 reverse phase column, respectively. The mobile phase composition and electrospray parameters are described in (Giavalisco et al., 2009). Chromatograms were recorded in survey MS mode (Mass Range [100 - 1500]) for hydrophilic compounds and in DDA MS/MS (40 eV collision energy) mode for lipophilic compounds. GC-MS measurements were performed as follows. An aliquot of lower polar extraction phase was dried and the dry residue was sequentially derivatized by methoxyamine/MSTFA and injected onto DB35 GC column (Agilent Technologies GC machine) coupled to Leco Pegasus HT mass spectrometer with EI ionization source. Gas elution was performed for two minutes at 85 °C with a further temperature gradient of 15 °C per minute untill a final temperature of 360 °C was reached.

Peak-picking and background removal of the LC-MS data from measurements of hydrophilic extraction phase was accomplished with the Genedata REFINER MS® 7.5 software. Chromatogram alignment and filtering were completed using in-house R-based software. Filtering included removal of isotopic peaks, in-source fragments, and additional lower intense adducts of the same analyte. The annotation of the content of the sample was accomplished by matching the extracted data from the chromatograms with our library of reference compounds in terms of accurate mass and retention time, and the most abundant adduct was used for relative quantification of a metabolite. For GC-MS data of the same extraction phase NetCDF files were exported from the Leco Pegasus software to "R". The package TargetSearch was used to transform retention time to retention index (RI), to align the chromatograms, extract the peaks, and annotate them by comparing the spectra and the RI to the Golm metabolome database. A unique mass was used to relatively quantify each identified metabolite. For those metabolites, which were annotated in both GC-MS and LC-MS data the value with smallest deviation was kept.

Peak-picking of the LC-MS/MS data from measurements of the lipophilic extraction phase was accomplished with the Genedata REFINER MS® 7.5 software without alignment. Identification of lipid species was performed using output.mgf files with dedicated in-house R-based software. Acyl composition of di- and triacylglycerols was established from the [Acyl + NH4] neutral loss in positive ion mode using a pre-formed library of accurate masses for all possible precursor and fragment peaks.

Mitochondrial respiration

10 mg (wet weight) of BAT were minced and incubated in Mir05 with 50 µg/mL Saponin for 30 min at 37 °C to permeabilize the cell membrane. Mir05 is composed of 0.5 mM EGTA, 3 mM $MgCl_2$, 60 mM K-lactobionate, 20 mM Taurine, 10 mM KH_2PO_4, 20 mM HEPES, 110 mM Sucrose, and 1 g/L BSA fatty acid free. Respiration of permeabilized brown adipocytes was measured by high-resolution respiratory using Oxygraph-2K (OROBOROS INSTRUMENTS, Innsburk, Austria) at 37 °C in 2 mL glass chambers. For each experiment, one control mouse and one $Lsd1^{cKO}$ mouse were processed in parallel in the 2 chambers. Mitochondrial respiration was assessed in Mir05 buffer supplemented with 5 mM glutamate and 2 mM malate substrates to activate mitochondrial complex I. After stabilization of mitochondrial respiration, 10 mM succinate were added to activate complex II. Maximal respiration rate was then recorded. 0.5 µM rotenone were finally added to inactivate mitochondrial complex I and measure complex II specific activity. Respiration rates were expressed in pmol / s and reported to 1 mg of tissue. Results presented correspond to maximal mitochondrial respiration rate. Alternatively, mitochondrial respiration was analyzed using 100 µM palmitoyl-L-carnitin as substrate.

Supplemental References

Ashburner, M., Ball, C.A., Blake, J.A., Botstein, D., Butler, H., Cherry, J.M., Davis, A.P., Dolinski, K., Dwight, S.S., Eppig, J.T.*, et al.* (2000). Gene ontology: tool for the unification of biology. The Gene Ontology Consortium. Nat Genet *25*, 25-29.

Bookout, A.L., Cummins, C.L., Mangelsdorf, D.J., Pesola, J.M., and Kramer, M.F. (2006). High-throughput real-time quantitative reverse transcription PCR. Curr Protoc Mol Biol *Chapter 15*, Unit 15 18.

Duteil, D., Metzger, E., Willmann, D., Karagianni, P., Friedrichs, N., Greschik, H., Gunther, T., Buettner, R., Talianidis, I., Metzger, D.*, et al.* (2014). LSD1 promotes oxidative metabolism of white adipose tissue. Nat Commun *5*, 4093.

Giavalisco, P., Kohl, K., Hummel, J., Seiwert, B., and Willmitzer, L. (2009). 13C isotope-labeled metabolomes allowing for improved compound annotation and relative quantification in liquid chromatography-mass spectrometry-based metabolomic research. Anal Chem *81*, 6546-6551.

Heinz, S., Benner, C., Spann, N., Bertolino, E., Lin, Y.C., Laslo, P., Cheng, J.X., Murre, C., Singh, H., and Glass, C.K. (2010). Simple combinations of lineage-determining transcription factors prime cis-regulatory elements required for macrophage and B cell identities. Mol Cell *38*, 576-589.

Langmead, B., Trapnell, C., Pop, M., and Salzberg, S.L. (2009). Ultrafast and memory-efficient alignment of short DNA sequences to the human genome. Genome Biol *10*, R25.

Metzger, E., Imhof, A., Patel, D., Kahl, P., Hoffmeyer, K., Friedrichs, N., Müller, J.M., Greschik, H., Kirfel, J., Ji, S.*, et al.* (2010). Phosphorylation of histone H3T6 by PKCbeta(I) controls demethylation at histone H3K4. Nature *464*, 792-796.

Metzger, E., Willmann, D., McMillan, J., Forne, I., Metzger, P., Gerhardt, S., Petroll, K., von Maessenhausen, A., Urban, S., Schott, A.K.*, et al.* (2016). Assembly of methylated KDM1A and CHD1 drives androgen receptor-dependent transcription and translocation. Nat Struct Mol Biol *23*, 132-139.

Metzger, E., Yin, N., Wissmann, M., Kunowska, N., Fischer, K., Friedrichs, N., Patnaik, D., Higgins, J.M., Potier, N., Scheidtmann, K.H.*, et al.* (2008). Phosphorylation of histone H3 at threonine 11 establishes a novel chromatin mark for transcriptional regulation. Nat Cell Biol *10*, 53-60.

Thorvaldsdottir, H., Robinson, J.T., and Mesirov, J.P. (2012). Integrative Genomics Viewer (IGV): high-performance genomics data visualization and exploration. Brief Bioinform.

Wang, J., Duncan, D., Shi, Z., and Zhang, B. (2013). WEB-based GEne SeT AnaLysis Toolkit (WebGestalt): update 2013. Nucleic Acids Res *41*, W77-83.

Wu, J., Bostrom, P., Sparks, L.M., Ye, L., Choi, J.H., Giang, A.H., Khandekar, M., Virtanen, K.A., Nuutila, P., Schaart, G.*, et al.* (2012). Beige adipocytes are a distinct type of thermogenic fat cell in mouse and human. Cell *150*, 366-376.

Zhang, Y., Liu, T., Meyer, C.A., Eeckhoute, J., Johnson, D.S., Bernstein, B.E., Nusbaum, C., Myers, R.M., Brown, M., Li, W.*, et al.* (2008). Model-based analysis of ChIP-Seq (MACS). Genome Biol *9*, R137.

Zhu, D., Holz, S., Metzger, E., Pavlovic, M., Jandausch, A., Jilg, C., Galgoczy, P., Herz, C., Moser, M., Metzger, D.*, et al.* (2014). Lysine-specific demethylase 1 regulates differentiation onset and migration of trophoblast stem cells. Nat Commun *5*, 3174.